

Interaction Energies of Generalised Monopoles

B. Kleihaus,^{*1} D. O’Keeffe^{*} and D.H. Tchrakian^{*†}

^{*}*Department of Mathematical Physics, National University of Ireland, Maynooth,
Maynooth, Ireland*

[†]*School of Theoretical Physics, Dublin Institute for Advanced Studies,
10 Burlington Road, Dublin 4, Ireland.*

Abstract

Generalisations of the ’t Hooft-Polyakov monopole which can exhibit *repulsion* only, *attraction* only, and both *attraction* and *repulsion*, between like monopoles, are studied numerically. The models supporting these solitons are $SO(3)$ gauged Higgs models featuring Skyrme-like terms.

¹on leave of absence from Fachbereich Physik, Universität Oldenburg, D-26111 Oldenburg, Germany

1 Introduction

It is well known that 't Hooft-Polyakov [1, 2] monopoles of like magnetic charge repel. For all finite values of the Higgs mass, or the coupling constant of the Higgs self-interaction potential, like monopoles exhibit a single repulsive phase only. This is understood as follows: In the Prasad-Sommerfield (PS) [3] limit, the Higgs field is massless and hence mediates a long range attractive force that cancels the long range repulsive magnetic force of the $U(1)$ field, exactly. In this limit, all components of the stress tensor vanish [4] resulting in the vanishing of inter-monopole forces. The force between like monopoles in the BPS limit was studied in detail by Manton [5] and Nahm [6], who showed that it decreases faster than any inverse power. In the presence of the usual Higgs potential however, the Higgs field becomes massive and as a result decays exponentially. Consequently the long range magnetic field dominates at large distances, leading to the repulsion of like monopoles of the Georgi-Glashow (GG) model. This was also concluded by Goldberg et al. [7], using the time-rate of change of the stress tensor for the field configuration of two exponentially localized monopoles, situated apart at a distance much larger than the sizes of the monopole cores. Recently Kiselev and Shnir [8] also have shown this employing the fluctuations and zero modes around the monopoles. That there is only one repulsive phase has been verified in [9], by calculating the energy *per unit topological charge* for a charge-2 and charge-1 solution numerically for all values of the Higgs potential coupling constant. The procedure in Ref. [9] is exactly analogous to that adopted by Jacobs and Rebbi [10] in their investigation of attractive and repulsive phases in the Abelian Higgs model.

Implementing the procedure of Ref. [10] in our 3 dimensional context necessitates the numerical solution of the partial differential equations of the axially symmetric fields. This is because the charge-2 monopole in 3 dimensions is not spherically symmetric, unlike in the case of the 2 dimensional context of the Abelian Higgs model [10] and of the hierarchy of Abelian Higgs models [11], where vorticity- n solutions are radially symmetric and hence result from ordinary differential equations. Thus, one of the most important technical ingredients of this work is the imposition of the axial symmetry on the $SO(3)$ gauge field and the algebra valued Higgs, for which we use the Ansatz of Rebbi and Rossi [12].

The purpose of the present work is to show that certain generalisations of the monopoles of the GG model, exhibit (a) a *repulsive* phase only like the usual monopole, (b) an *attractive* only, and (c) both *attractive* and *repulsive* phases. This is done by integrating the Euler-Lagrange equations arising from the static Hamiltonians of the new models, numerically, in exact analogy with the procedures used in Refs. [10, 9]. The models under consideration, just like the GG model, are 3 dimensional $SO(3)$ Higgs models. These models are constructed from the hierarchy of 3 dimensional $SO(3)$ Higgs models, obtained by dimensional descent from the $4p$ dimensional hierarchy of chiral $SO(4p)$ Yang-Mills models [13]¹. Here, we will restrict to the $p = 1$

¹There are similar hierarchies of d dimensional $SO(d)$ Higgs models with $d < 4p$ [14]

and the $p = 2$ members of this hierarchy, of which the $p = 1$ member is nothing else than the PS limit of the GG model. Thus the main new ingredient in the models presented here will be the $p = 2$ model, whose spherically symmetric monopole solutions were studied numerically in our previous work [15], to which we shall refer for certain details later.

In Ref. [15], we have discussed the charge-1 solutions of the $p = 2$ model in some detail, especially with regard to its properties relative to the GG and the Abelian Higgs models. There we have pointed out that the $p = 2$ model does not support self-dual solutions. However, for certain values of the coupling constants it nevertheless supports a solution whose energy is quantitatively extremely close to the Bogomol'nyi lower bound, and correspondingly, an estimate of some components of the stress tensor indicates that the force on the soliton is also extremely small. We described such a solution as being “almost self-dual” and we designated the corresponding values of the coupling constants as *critical*. This is in accordance with the usual nomenclature whereby the Bogomol'nyi inequalities are saturated for the *critical* values of the coupling constants in a given model. It is important to recall [14, 15] that the *critical* dimensionless coupling constants of the $p = 2$ model take *nonzero* values. In this sense the $p = 2$ model is similar to the Abelian Higgs model, which supports a self-dual solution for a finite value of the dimensionless coupling constant, and it is in contrast to the GG model for which the critical value of the (Higgs) coupling constant *vanishes*. Hence it was argued in Ref. [15] that like the Abelian Higgs model, the 3 dimensional $p = 2$ $SO(3)$ Higgs model, supports both attractive and repulsive phases.

To put all this in perspective, we note that there is a difference between the $p = 2$ model on the one hand and the $p = 1$ and the abelian Higgs model on the other hand. In the latter, the Bogomol'nyi inequality is saturated at the *critical* coupling constants for all topological charges n . Thus the *critical* values of the coupling constants characterise a property of the model itself. For the $p = 2$ model we only know that for the charge-1 solution the energy is close to the Bogomol'nyi bound at the *critical* coupling constants. If these coupling constants characterise the model, and not only a single solution, then the energy of all charge- n solutions should be near their Bogomol'nyi bounds at the same values of the coupling constants. So we do not specify quantitatively what we mean by ‘near the Bogomol'nyi bound’, there might be a subset of values of the coupling constants which can be called *critical*. For the charge-2 solution of the $p = 2$ model we expect that the energy will be near the Bogomol'nyi bound for coupling constants close to the *critical* coupling constants determined by the investigation of the charge-1 solutions. If this is the case, attractive and repulsive phases possibly exist with a crossover at values of the coupling constants near the *critical* values.

It is one of the aims of the present work to verify this hypothesis. This will be done by straightforwardly integrating the Euler-Lagrange equations numerically on the charge-1 and charge-2 sectors. Thus the argument based on the *almost self-duality* of the $p = 2$ monopoles, that makes the existence of the two phases plausible, will not be further elaborated here, and we refer to Refs. [11, 15] for that.

In general, our aim is to present all the generalised $SO(2)$ Higgs models with Hamiltonian densities carrying dimensions up to L^{-8} , which includes of course the GG model with dimension L^{-4} . Note that the limitation we impose is a consequence of limiting our study to the $p = 2$ model, whose Hamiltonian density has the dimensions L^{-8} . The inclusion of the GG or the $p = 1$ model results in the presence of the usual Yang-Mills term and hence in the possibility of describing free gauge fields, absent in the pure $p = 2$ (and $p \geq 2$) model(s). We note that the $p \geq 2$ models are purely Skyrme-like gauged Higgs systems [16] in the sense that they consist of $2p$ th powers of the curvature and covariant derivative, suitably antisymmetrised so that only the squares of velocity-fields appear. In this sense, the composite models consisting of the $p = 1$ model augmented by $p \geq 2$ models, are quite analogous to the Skyrme model [17] where the latter terms play the role of the Skyrme term of the $O(4)$ sigma model.

It is worthwhile making some clarifications concerning the construction of the composite models. We know from the results and the arguments of Refs. [11, 15] that we would expect a phase change from attractive to repulsive, to take place at the *almost self-dual* configurations of the systems. The composite models however are even less self-dual than the $p = 1$ and the $p = 2$ modes on their own, since the Bogolmol'nyi equations are even more overdetermined than those of the $p = 2$ model on its own and hence the solutions of the composite models are more remote from saturating the Bogolmol'nyi bound. (Clearly, exact self-dual solutions can be achieved if we suppress the entire $p = 2$ content of the model, but then there will be no interactions between the monopoles. Since our aim is to produce a (composite) model accomodating interactions, we will resist on retaining some or all of the components of the $p = 2$ model.) We will investigate three possibilities, (a) when the $p = 1$ system dominates, which can be regarded as a $p = 1$ model extended with a $p = 2$ Skyrme-term, (b) when the two constituents of the composite model are equally important, and (c) when the $p = 2$ model dominates, which yields the pure $p = 2$ model whose spherically symmetric solutions were studied in Ref. [15]. We shall study all these three cases in this work.

In Section 2 we define the static Hamiltonians of the various models we will study and proceed in Section 3 to state the axially symmetric Ansatz of Rebbi and Rossi [12], leading to the residual 2 dimensional subsystems of the models introduced in the previous section. In Sections 4, 5 and 6, we present the results of the numerical computations, respectively for the extended $p = 1$ models where the latter dominates, the composite $p = 1$ and $p = 2$ system, and the pure $p = 2$ system which is the limiting case of the composite system where the $p = 2$ dominates. Our choice for this order of presentation is the result of the successively increasing complication involved in the numerical computations involved in each of these cases, so that we have chosen to tackle the most easily accessible cases first. Section 7, finally, is devoted to the summary and discussion of the results.

2 The Models

Since various aspects of the 3 dimensional hierarchy of $SO(3)$ gauged Higgs models are discussed in detail in Refs. [14, 15, 16], we shall restrict ourselves here to the definitions of the Hamiltonian densities only. We refer to Refs. [14, 16] for their construction, as well as the topological inequalities, via dimensional descent. For the detailed normalisation of the topological charge and the asymptotic properties required by the finite energy condition and analyticity, we refer to Ref. [15].

Below, we shall denote the gauge and Higgs fields

$$A_i = -\frac{i}{2}A_i^a\sigma_a, \quad \phi = -\frac{i}{2}\phi^a\sigma_a \quad (1)$$

in an antihermitian notation. The resulting antihermitian curvature and covariant derivative are then

$$F_{ij} = \partial_i A_j - \partial_j A_i + [A_i, A_j], \quad (2)$$

$$D_i\phi = \partial_i\phi + [A_i, \phi]. \quad (3)$$

2.1 The $p = 1$ model

This is the PS limit of the GG model, characterised by the static Hamiltonian

$$\mathcal{H}^{(1)} = \text{Tr}\left(\frac{1}{4}F_{ij}F^{ij} + \frac{1}{2}D_i\phi D^i\phi\right). \quad (4)$$

The reason that we have distinguished between covariant and contravariant indices is that in what follows we shall have occasion to use a spherical (not Cartesian) basis.

The system supports self-dual solutions saturating the topological lower bound [18], which equals the magnetic charge. This model is extensively studied since a long time and will not be considered in isolation here.

2.2 The $p = 2$ model

The static Hamiltonian of this model is [15]

$$\mathcal{H}^{(2)} = \frac{5}{18 \times 32} \sum_{A=1}^4 \lambda_A \mathcal{H}_A^{(2)}, \quad (5)$$

where each of the four densities $\mathcal{H}_A^{(2)}$ are defined by

$$\mathcal{H}_4^{(2)} = \text{Tr}\{F_{[ij}, D_{k]}\phi\}\{F^{[ij}, D^{k]}\phi\}, \quad (6)$$

$$\mathcal{H}_3^{(2)} = -6\text{Tr}(\{S, F_{ij}\} + [D_i\phi, D_j\phi])(\{S, F^{ij}\} + [D^i\phi, D^j\phi]), \quad (7)$$

$$\mathcal{H}_2^{(2)} = -27\text{Tr}\{[S, D_i\phi]\{S, D^i\phi\}\}, \quad (8)$$

$$\mathcal{H}_1^{(2)} = 54\text{Tr}S^4. \quad (9)$$

In (6)-(8), we have used $[ijk]$ to denote cyclic symmetry in the indices i, j, k , $\{A, B\}$ denotes an anticommutator, and

$$S = -(\eta^2 + \phi^2). \quad (10)$$

The reason that we have distinguished between covariant and contravariant indices in (6)-(9) is the same as in (4).

In (5) we can set $\lambda_4 = 1$ by scaling with an overall constant. (λ_4 is reserved for use only when we construct a composite model by combining the $p = 1$ and $p = 2$ models.) When the dimensionless coupling constants λ_1, λ_2 and λ_3 are restricted to their critical values $\lambda_1 = \lambda_2 = \lambda_3 = 1$, then the topological inequality

$$\int \mathcal{H}^{(2)}(\lambda_1 = \lambda_2 = \lambda_3 = 1) d^3r \geq 4\pi n \eta^5, \quad (11)$$

where n is the topological charge, can be saturated by the corresponding Bogomol'nyi equations. The latter being overdetermined [14] they do not support nontrivial solutions. Nevertheless there exist nontrivial solutions, that do not satisfy the Bogomol'nyi equations, with energies lying above but numerically very close to the Bogomol'nyi lower bound. The spherically symmetric solution found in Ref. [15] is of this type, described as being *almost self-dual*. When all the coupling constants are greater than 1, i.e. $\lambda_A \geq 1$, then the topological inequality (11) is preserved. When however any of the coupling constants takes a lower value than 1, i.e. $\lambda_A \leq 1$, then the inequality (11) is replaced by

$$\int \mathcal{H}^{(2)} d^3r \geq 4\pi \lambda_{min} n \eta^5, \quad (12)$$

where λ_{min} is the smallest of λ_A , $A = 1, 2, 3$.

From the results in Ref. [11], where we have seen that there is a crossover point between attractive and repulsive phases in the vicinity of the critical values of the dimensionless coupling constants of a system supporting *almost self-dual* solutions, we expect this to be the case also for the $p = 2$ model (5), which we know from the results of Ref. [15] that it does support *almost self-dual* solutions.

2.3 The composite model

By composite models we mean the system characterised by the sum of the static Hamiltonians $\mathcal{H}^{(p)}$, always including the $p = 1$ member of the hierarchy. Here we are limiting ourselves to $p = 1$ and $p = 2$. In **2.3.1**, we define the models we shall subsequently study numerically. In **2.3.2**, we estimate the dependence of the energy on the coupling constants λ_A in the region $\lambda_A \ll 1$.

2.3.1 The generic case

The Hamiltonian density of this model is

$$\mathcal{H}^{(c)} = \mathcal{H}^{(1)} + \eta^{-4} \mathcal{H}^{(2)}, \quad (13)$$

whose Bogomol'nyi lower bound is twice $4\pi n\eta$ if $\lambda_A \geq 1$.

In (13), the dimensionless coupling constants λ_A for all four $A = 1, 2, 3, 4$, can take on any positive definite values, and even when any or all λ_A vanish, the Bogomol'nyi lower bound does not sink to zero as for the $p = 2$ model in (12), since the energy of the $p = 1$ model is still bounded by the usual magnetic charge. The fact that it is possible to set all but one of the λ_A equal to zero in (13) leads us to describe (13) as an extended $p = 1$ model. For example if we set all but one λ_A in (13) equal to zero we have four special composite models, and if we set any two of them equal to zero we have six special composite models, etc. The first case is quite special. These four models are similar to the GG model insofar as they describe a $p = 1$ model with only one additional term. This suggests that like the GG model, these four composite models support only one phase, i. e. an attractive only or a repulsive one only. We shall give a strongly suggestive analytic argument for this in **2.3.2** below.

Since the Bogomol'nyi bounds of the solutions to (13) are more substantially exceeded than in the $p = 2$ model, here we cannot invoke the presence of almost self-dual solutions. Thus in the generic case, where λ_A are not considered to be small we cannot predict anything about the interaction of the monopoles. The situation is different however, when all $\lambda_A \ll 1$. In these cases it is possible to examine this question systematically as we shall do in the following subsections.

In order to determine whether there is a repulsive phase, an attractive phase or a crossover we follow Jacobs and Rebbi [10], and define the difference of the energy *per unit topological charge* for the charge-2 and charge-1 solutions at fixed coupling constants λ_A ,

$$\Delta E(\lambda_A) \stackrel{def.}{=} \frac{E^{(2)}(\lambda_A)}{2} - E^{(1)}(\lambda_A), \quad (14)$$

where $E^{(n)}(\lambda_A)$ is the energy of the charge- n solution. The monopoles repel when $\Delta E(\lambda_A) > 0$ and attract when $\Delta E(\lambda_A) < 0$. If the quantity $\Delta E(\lambda_A)$ vanishes, we find a crossover at λ_A .

2.3.2 Perturbed $p = 1$ models

What is very interesting about the extended models is, that the behaviour of the solutions on the constants λ_A can be analytically estimated for small values of the coupling constants, $\lambda_A \ll 1$. We shall restrict, at first, to the case where there is only one nonzero λ_A in $\mathcal{H}^{(2)}$.

Consider the energy integral

$$E^{(n)}(\lambda_A) = \int (\mathcal{H}^{(1)} + \frac{5}{18 \times 32} \eta^{-4} \lambda_A \mathcal{H}_A^{(2)}) d^3x, \quad (15)$$

as a function of λ_A . The energy density functional in (15) is the special case of the composite static Hamiltonian (13) in which all but a given coupling constant λ_A are set equal to zero, and is evaluated for the topological charge- n solution described by the fields $(A_i^{(\lambda_A)}, \phi^{(\lambda_A)})$.

We now insist that $\lambda_A \ll 1$, and make a Taylor expansion of $E^{(n)}(\lambda_A)$,

$$E^{(n)}(\lambda_A) = E^{(n)}(0) + \lambda_A \left. \frac{dE^{(n)}}{d\lambda_A} \right|_{\lambda_A=0} + o(\lambda_A^2). \quad (16)$$

Because $\lambda_A \ll 1$, we can describe the solution fields in the energy density functional in (15) as small perturbations of the known charge- n PS [3] solution fields $(A_i^{(0)}, \phi^{(0)})$

$$A_i^{(\lambda_A)} = A_i^{(0)} + \lambda_A a_i, \quad \phi^{(\lambda_A)} = \phi^{(0)} + \lambda_A \varphi \quad (17)$$

in terms of the functions (a_i, φ) which in principle can be found.

The first term in the Taylor expansion (16) is recognised as the energy of the PS solution, and equals $4\pi n\eta$. To calculate the second term, we differentiate the energy integral (15), which involves the differentiation of the functional in the integrand both with respect to its implicit dependence on λ_A through the fields $A_i^{(\lambda_A)}, \phi^{(\lambda_A)}$, and its explicit dependence. The terms arising from the differentiation of the implicit dependence on λ_A amount to subjecting the functional $\mathcal{H}^{(1)} + \frac{5}{18 \times 32} \eta^{-4} \lambda_A \mathcal{H}^{(2)}$ to the variational principle, which vanish by virtue of the Euler-Lagrange equations satisfied by the solution fields (17). The result of the differentiation with respect to the explicit dependence on λ_A then is the only contribution

$$\frac{dE^{(n)}}{d\lambda_A} = \frac{5}{18 \times 32} \eta^{-4} \int \mathcal{H}_A^{(2)}[A_i^{(\lambda_A)}, \phi^{(\lambda)}] d^3x, \quad (18)$$

which evaluated at $\lambda_A = 0$ is

$$\left. \frac{dE^{(n)}}{d\lambda_A} \right|_{\lambda_A=0} = \frac{5}{18 \times 32} \eta^{-4} \int \mathcal{H}_A^{(2)}[A_i^{(0)}, \phi^{(0)}] d^3x, \quad (19)$$

an integral evaluated strictly in terms of the PS solution fields $(A_i^{(0)}, \phi^{(0)})$. This is the sense in which the present calculation is described as being *perturbative*.

Refining our notation for the PS solution fields $(A_i^{(0)}, \phi^{(0)})$ by labeling them further with the topological charge n as $(A_i^{(0)}(n), \phi^{(0)}(n))$, we substitute (19) in (14)

$$\begin{aligned} \Delta E &= c_A \lambda_A \\ c_A &= \frac{5}{18 \times 32} \eta^{-4} \left(\frac{1}{2} \int \mathcal{H}_A^{(2)}[A_i^{(0)}(2), \phi^{(0)}(2)] d^3x - \int \mathcal{H}_A^{(2)}[A_i^{(0)}(1), \phi^{(0)}(1)] d^3x \right) \end{aligned} \quad (20)$$

Clearly, when the quantity c_A in (20) is positive (negative) the monopoles repel (attract). Moreover, if we assume that the dependence of the energies on λ_A is monotonic, then this will be the only phase, like in the GG model. It is important however to stress that the above arguments do not apply to the GG model, namely, that the GG model cannot be treated as a perturbation of the $p = 1$ (BPS) system [9].

In table 1 the values of $\left. \frac{1}{n} \frac{dE^{(n)}}{d\lambda_A} \right|_{\lambda_A=0}$ for the charge-1 and the charge-2 solutions and c_A are given. Note, c_A , $A = 2, 3, 4$ are of the same order of magnitude, whereas

c_1 is more than one order of magnitude larger. c_1 and c_2 are positive, leading to repulsion of like monopoles for the models with $\lambda_1 \neq 0$ or $\lambda_2 \neq 0$. For the models with $\lambda_3 \neq 0$ or $\lambda_4 \neq 0$ the constants c_3 and c_4 are negative. Hence these models have only attractive phases.

The above perturbative argument can be systematically extended to the case of the full composite model with all or some of the $\lambda_A \neq 0$. The only difference there will be that the Taylor expansion will have more than one contribution (one from each nonzero λ_A),

$$\Delta E = \sum_{A=1}^4 c_A \lambda_A . \tag{22}$$

Indeed, it would be expected that there should be both phases, like in the generic case. If at least two of the constants c_A have opposite signs then the model has attractive and repulsive phases. The change of the phases occurs for the values of the parameters λ_A for which ΔE becomes zero. This is verified by our numerical studies for small values of λ_A , reported later.

3 Axial Symmetry

Imposition of axial symmetry proceeds readily by the application of the Rebbi-Rossi Ansatz [12]. When subjected to axial symmetry, the 12 fields consisting of the 3 components of the isospin-1 gauge field and the isospin-1 Higgs field are parametrised by 6 functions. It is instructive to describe [19, 12] these 6 functions as a 2 component real field \mathcal{A}_μ , with $\mu = 1, 2$ labeling the 2 dimensional coordinate $\xi_\mu = r, z$, $r = \sqrt{x^2 + y^2}$, and two complex scalar fields φ and χ . In this parametrisation, all Lorentz and $SU(2)$ gauge invariant Hamiltonian densities $\mathcal{H}^{(p)}$ reduce to an Abelian Higgs model in which \mathcal{A}_μ plays the role of a $U(1)$ connection, and the two complex scalar fields φ and χ play the roles of Higgs fields. The asymptotic behaviours required of these functions φ and χ by the requirements of finite energy and analyticity are typical of Higgs fields, hence justifying the description of the axially symmetric 2 dimensional reduced subsystems of the p -th $SO(3)$ gauged Higgs model in 3 dimensions, as residual Abelian two-Higgs models in 2 dimensions. (In particular, one of the complex fields, say φ actually is endowed with a Higgs type self-interaction potential, and the two Higgs fields exhibit a Yukawa-type mutual interaction term.) Given that the residual subsystem exhibits a $U(1)$ gauge symmetry, it is necessary to remove one of the 6 residual fields by fixing this gauge. The natural choice we will make here, which has been used previously in Refs. [20, 21], is

$$\partial_\mu \mathcal{A}_\mu = 0, \tag{23}$$

which we call a Coulomb gauge as before [20, 21].

In the following, we shall not describe the axially symmetric subsystem in terms of the functions $(\mathcal{A}_\mu, \varphi, \chi)$, but will use rather another parametrisation formulated in spherical coordinates. This choice is made because it enables the efficient imposition of the boundary conditions in the numerical computations to follow.

First we define the $su(2)$ matrices $\tau_a^{(n)}$ in terms of Pauli matrices σ_a and spatial coordinates θ, φ

$$\tau_r^{(n)} = \sin \theta \cos n\varphi \sigma_1 + \sin \theta \sin n\varphi \sigma_2 + \cos \theta \sigma_3 , \quad (24)$$

$$\tau_\theta^{(n)} = \cos \theta \cos n\varphi \sigma_1 + \cos \theta \sin n\varphi \sigma_2 - \sin \theta \sigma_3 , \quad (25)$$

$$\tau_\varphi^{(n)} = -\sin n\varphi \sigma_1 + \cos n\varphi \sigma_2 , \quad (26)$$

where n is the winding number. For the Ansätze of the gauge field and the Higgs field we impose axial symmetry and in addition parity reflection symmetry. Using spherical coordinates the Ansatz of the gauge field

$$A_i dx^i = A_r dr + A_\theta d\theta + A_\varphi d\varphi \quad (27)$$

can be parametrized by four functions $H_k(r, \theta)$,

$$A_r = \frac{H_1(r, \theta)}{r} \frac{i\tau_\varphi^{(n)}}{2} , \quad A_\theta = (1 - H_2(r, \theta)) \frac{i\tau_\varphi^{(n)}}{2} , \quad (28)$$

$$A_\varphi = -n \sin \theta (H_3(r, \theta) \frac{i\tau_r^{(n)}}{2} + (1 - H_4(r, \theta)) \frac{i\tau_\theta^{(n)}}{2}) . \quad (29)$$

The Ansatz for the Higgs field can be parametrised by two functions $\phi_k(r, \theta)$

$$\frac{1}{2}\phi = \phi_1(r, \theta) \frac{i\tau_r^{(n)}}{2} + \phi_2(r, \theta) \frac{i\tau_\theta^{(n)}}{2} . \quad (30)$$

Expanding the curvature tensor F_{ij} in terms of the matrices $i\tau_a^{(n)}/2$,

$$F_{ij} = F_{ij}^{(a)} \frac{i\tau_a^{(n)}}{2} , \quad (31)$$

we find for the non-vanishing coefficients $F_{ij}^{(a)}$,

$$F_{r\theta}^{(\varphi)} = -\frac{1}{r}(r\partial_r H_2 + \partial_\theta H_1) , \quad (32)$$

$$F_{r\varphi}^{(r)} = -\frac{n}{r} \sin \theta (r\partial_r H_3 - H_1 H_4) , \quad (33)$$

$$F_{r\varphi}^{(\theta)} = \frac{n}{r} \sin \theta (r\partial_r H_4 + H_1 (H_3 + \cot \theta)) , \quad (34)$$

$$F_{\theta\varphi}^{(r)} = -n \sin \theta (\partial_\theta H_3 + H_3 \cot \theta + H_2 H_4 - 1) , \quad (35)$$

$$F_{\theta\varphi}^{(\theta)} = n \sin \theta (\partial_\theta H_4 + (H_4 - H_2) \cot \theta - H_2 H_3) . \quad (36)$$

Similarly we find for the expansion of the covariant derivative of the Higgs field,

$$D_\mu\phi = (D_\mu\phi)^{(a)} \frac{i\tau_a^{(n)}}{2} , \quad (37)$$

the non-vanishing coefficients

$$(D_r\phi)^{(r)} = \frac{1}{r}(r\partial_r\phi_1 + H_1\phi_2) , \quad (38)$$

$$(D_r\phi)^{(\theta)} = \frac{1}{r}(r\partial_r\phi_2 - H_1\phi_1) , \quad (39)$$

$$(D_\theta\phi)^{(r)} = \partial_\theta\phi_1 - H_2\phi_2 , \quad (40)$$

$$(D_\theta\phi)^{(\theta)} = \partial_\theta\phi_2 + H_2\phi_1 , \quad (41)$$

$$(D_\varphi\phi)^{(\varphi)} = n\sin\theta(\phi_1 H_4 + \phi_2(H_3 + \cot\theta)) . \quad (42)$$

With these Ansätze the Hamiltonian densities eqs. (6)-(9) can be expressed as

$$\begin{aligned} \mathcal{H}_4^{(2)} &= 3 \left[F_{r\theta}^{(\varphi)} (D_\varphi\phi)^{(\varphi)} \right. \\ &\quad + F_{\varphi r}^{(r)} (D_\theta\phi)^{(r)} + F_{\varphi r}^{(\theta)} (D_\theta\phi)^{(\theta)} \\ &\quad \left. + F_{\theta\varphi}^{(r)} (D_r\phi)^{(r)} + F_{\theta\varphi}^{(\theta)} (D_r\phi)^{(\theta)} \right]^2 \frac{1}{\sin^2\theta r^4} , \end{aligned} \quad (43)$$

$$\begin{aligned} \mathcal{H}_3^{(2)} &= 6 \left\{ \frac{1}{r^2} \left[2(\eta^2 - \frac{1}{4}(\phi_1^2 + \phi_2^2)) F_{r\theta}^{(\varphi)} + (D_r\phi)^{(r)}(D_\theta\phi)^{(\theta)} - (D_r\phi)^{(\theta)}(D_\theta\phi)^{(r)} \right]^2 \right. \\ &\quad + \frac{1}{\sin^2\theta r^2} \left[2(\eta^2 - \frac{1}{4}(\phi_1^2 + \phi_2^2)) F_{\varphi r}^{(r)} + (D_\varphi\phi)^{(\theta)}(D_r\phi)^{(\varphi)} \right]^2 \\ &\quad + \frac{1}{\sin^2\theta r^2} \left[2(\eta^2 - \frac{1}{4}(\phi_1^2 + \phi_2^2)) F_{\varphi r}^{(\theta)} - (D_\varphi\phi)^{(r)}(D_r\phi)^{(\varphi)} \right]^2 \\ &\quad + \frac{1}{\sin^2\theta r^4} \left[2(\eta^2 - \frac{1}{4}(\phi_1^2 + \phi_2^2)) F_{\theta\varphi}^{(r)} + (D_\theta\phi)^{(\theta)}(D_\varphi\phi)^{(\varphi)} \right]^2 \\ &\quad \left. + \frac{1}{\sin^2\theta r^4} \left[2(\eta^2 - \frac{1}{4}(\phi_1^2 + \phi_2^2)) F_{\theta\varphi}^{(\theta)} - (D_\theta\phi)^{(r)}(D_\varphi\phi)^{(\varphi)} \right]^2 \right\} , \end{aligned} \quad (44)$$

$$\begin{aligned} \mathcal{H}_2^{(2)} &= 54(\eta^2 - \frac{1}{4}(\phi_1^2 + \phi_2^2))^2 \left\{ [(D_r\phi)^{(r)}]^2 + [(D_r\phi)^{(\theta)}]^2 \right. \\ &\quad \left. + \frac{1}{r^2} \left([(D_\theta\phi)^{(r)}]^2 + [(D_\theta\phi)^{(\theta)}]^2 \right) + \frac{1}{\sin^2\theta r^2} [(D_\varphi\phi)^{(r)}]^2 \right\} , \end{aligned} \quad (45)$$

$$\mathcal{H}_1^{(2)} = 108 \left[\eta^2 - \frac{1}{4}(\phi_1^2 + \phi_2^2) \right]^4 , \quad (46)$$

respectively.

With the Ansatz of the gauge fields we express the gauge constraint eq. (23) in the form

$$G_c = \frac{1}{r}(\partial_r H_1 - \frac{1}{r}\partial_\theta H_2) = 0 . \quad (47)$$

The variational equations are to be derived from the Hamiltonians of the models with the term $\mu_L G_c^2$ added, where μ_L is the Lagrange multiplier.

For $n = 1$ the spherically symmetric Ansatz is recovered with $H_1(r, \theta) \equiv H_3(r, \theta) \equiv \phi_2(r, \theta) \equiv 0$ and $H_2(r, \theta) \equiv H_4(r, \theta) = f(r)$, $\phi_1(r, \theta) = h(r)$, where $f(r)$, $h(r)$ are defined in [15].

The boundary conditions follow from the requirements of finite energy and analyticity as well as symmetry. They are given by

$$\begin{array}{ccc} & \text{at the origin} & \text{at infinity} \\ H_1(0, \theta) & = H_3(0, \theta) = 0 & H_k(\infty, \theta) = 0 \\ H_2(0, \theta) & = H_4(0, \theta) = 1 & \\ \phi_1(0, \theta) & = \phi_2(0, \theta) = 0 & \phi_1(\infty, \theta)/2\eta = 1 \end{array} \quad (48)$$

$$\begin{array}{ccc} & \text{on the } z\text{-axis} & \text{on the } \rho\text{-axis} \\ H_1(r, 0) & = H_3(r, 0) = 0 & H_1(r, \frac{\pi}{2}) = H_3(r, \frac{\pi}{2}) = 0 \\ \partial_\theta H_2(r, 0) & = \partial_\theta H_4(r, 0) = 0 & \partial_\theta H_2(r, \frac{\pi}{2}) = \partial_\theta H_4(r, \frac{\pi}{2}) = 0 \\ \phi_2(r, 0) & = \partial_\theta \phi_1(r, 0) = 0 & \phi_2(r, \frac{\pi}{2}) = \partial_\theta \phi_1(r, \frac{\pi}{2}) = 0 \end{array}$$

4 Numerical results

This Section deals with the results of the numerical integrations. The topological charge-1 and charge-2 solutions of the systems under consideration will be found numerically and the energies *per unit topological charge* of these solitons will be calculated as functions of the dimensionless coupling constants λ_A with the aim of deducing the presence of attractive and repulsive phases as the case may be, following the procedure of Ref. [10]. This will be done by holding all but one of the dimensionless coupling constants constant and varying the last one only, although, given that our models are characterised with more than one such constant, it would be possible to vary more than one of these at a time. This we do not do here. The present Section consists of three subsections.

The first subsection is concerned with certain extended $p = 1$ models. Of these the first is the GG model, while the next five are perturbative extensions of the $p = 1$ model which were described in Section 2.3.2 as perturbed $p = 1$ composite models consisting of the $p = 1$ model and all or some of the terms in the $p = 2$ model. The latter therefore differ from the GG model in two respects. Firstly, they incorporate terms from the $p = 2$ model which the GG model does not, and secondly, these terms may be regarded as perturbations of the $p = 1$ system unlike the GG model as explained in Section 2.3.2 and in Ref. [9]. In particular, we have studied the $p = 1$

model extended by each of the four terms constituting the $p = 2$ model, separately. The interest in these (perturbative) models is that according to our analysis in section 2.3.2 the attraction or repulsion of two like monopoles is decided by the slope of the energy versus the λ_A in question, and assuming quite reasonably that these curves are monotonic, this yields systems supporting only an attractive phase, or only a repulsive one. In addition to these four examples, we have studied the case of two nonvanishing λ_A , each chosen such that in the previous analysis the model with that particular λ_A supported, respectively, an attractive and a repulsive phase. In such a case, it is intuitively expected that the combined terms will result in a model supporting both phases, and since both λ_A are very small, the crossover point of the two phases is expected to be very near $\lambda_A = 0$, the critical value of the model, which in this case coincides with the critical value of the PS model.

The second subsection deals with the generic case of the composite model, i.e. that in which the values of the coupling constants λ_A are not small, so that this is not a perturbative extension of the $p = 1$ model. We will set three of the four dimensionless coupling constants λ_A equal to 1 and varying the fourth one. The main interest in these models is the question as to what phases are supported, the models themselves not being as closely *almost self-dual* as the $p = 2$ model on its own. For that reason it is not so easy to predict where, if anywhere, the crossover points will be situated. The other, technical, interest in the full composite model is that it affords us with an approach to the numerical integration of the $p = 2$ model on its own, by gradually decreasing its $p = 1$ content.

The third subsection deals exclusively with the $p = 2$ model, which from the viewpoint of numerical integrations is the most difficult of the models considered here.

The partial differential equations are solved numerically using the iterative Newton-Raphson method [22]. The calculations are performed with the rescaled Higgs field functions $\phi_1(r, \theta)/\eta$, $\phi_2(r, \theta)/\eta$. We employed the compactified dimensionless radial coordinate $x = \eta r/(1 + \eta r)$ to map spatial infinity to the finite value $x = 1$. The differential equations are discretized on a non-equidistant grid in x and θ covering the integration region $0 \leq x \leq 1$, $0 \leq \theta \leq \pi/2$. Typical grids have sizes of 70×20 gridpoints. The error estimates are of the order 10^{-3} .

4.1 Extended $p = 1$ models

4.1.1 The Georgi-Glashow model

This is the best known extended $p = 1$ model, and has been extensively studied in the literature analytically. A thorough numerical study of this model was recently performed in [9] where it was confirmed that this system supports a repulsive phase only. We refer to [9] for the analysis of this model.

This system consists of the $p = 1$ model to which the usual symmetry breaking Higgs self-interaction potential is added. It is well known [6, 9] that the addition of the latter term cannot be regarded as a perturbation of the $p = 1$ model. In this

respect this model differs from the composite models following in the next sections.

In Fig. 1 we show the energy density of the charge-2 solution of the $p = 1$ model as a function of the coordinates $\rho = \eta r \sin \theta$ and $z = \eta r \cos \theta$. The energy density has its maximum on the ρ -axis and is monotonic decreasing on the z -axis. Thus its shape deviates considerably from spherical symmetry. The surfaces of equal energy density form spheres for large distances from the origin and doughnuts for distances more close to the origin. The Maximum of the energy density corresponds is located on a circle in the $x - y$ plane.

4.1.2 $\lambda_4 = \lambda_3 = \lambda_2 = 0$ perturbed composite model

In this model only the potential term $\frac{5}{18 \times 32} \eta^{-4} \lambda_1 \mathcal{H}_1^{(2)}$ is added to the $p = 1$ model. In Fig. 2 the quantity $\Delta E(\lambda_1)$, as defined in eq. (14), is plotted as a function of the coupling constant λ_1 (solid line **a**) for $0 \leq \lambda_1 \leq 1$. $\Delta E(\lambda_1)$ is a monotonically increasing function. Consequently there is only a repulsive phase in this model.

The dashed straight line in Fig. 2 corresponds to the linear approximation of ΔE defined in eq. (20). The deviation of the function $\Delta E(\lambda_1)$ from this line occurs at rather small values of λ_1 . This shows that the linear approximation is valid only for very small values of λ_1 , roughly in the range $0 \leq \lambda_1 < 1/100$.

Note, that for this model the analysis of ref. [8] can be adopted. The reason is, that the actual form of the Higgs potential does not enter the analysis of the zero modes. Thus the conclusions of ref. [8] are valid for this model, too, provided the Higgs potential forces the Higgs field to decay faster than $1/r$.

4.1.3 $\lambda_4 = \lambda_3 = \lambda_1 = 0$ perturbed composite model

This model consists of the $p = 1$ model with only the term $\frac{5}{18 \times 32} \eta^{-4} \lambda_2 \mathcal{H}_2^{(2)}$ added to the $p = 1$ model. The quantity $\Delta E(\lambda_2)$ is shown in Fig. 2 as a function of λ_2 (solid line **b**). Again, $\Delta E(\lambda_2)$ is a monotonically increasing function. Thus there is only a repulsive phase in this model.

The dashed straight line shows the linear approximation of ΔE , eq. (20). For $\lambda_2 > 0.1$, ΔE deviates from this line. Therefore, the validity of the linear approximation to this model is restricted to the range $0 \leq \lambda_2 < 0.1$.

4.1.4 $\lambda_4 = \lambda_2 = \lambda_1 = 0$ perturbed composite model

This model consists of the $p = 1$ model with only the term $\frac{5}{18 \times 32} \eta^{-4} \lambda_3 \mathcal{H}_3^{(2)}$ added to the $p = 1$ model. This Skyrme like term leads to an attractive phase as can be seen from Fig. 2 (solid line **c**). $\Delta E(\lambda_3)$ is a monotonically decreasing function. The deviation from the linear approximation (dashed line) occurs at $\lambda_3 = 0.1$ implying that the validity of the linear approximation to this model is restricted to the range $0 \leq \lambda_3 < 0.1$.

4.1.5 $\lambda_3 = \lambda_2 = \lambda_1 = 0$ perturbed composite model

This model consists of the $p = 1$ model with only the term $\frac{5}{18 \times 32} \eta^{-4} \lambda_4 \mathcal{H}_4^{(2)}$ added. Again this model has only an attractive phase. The quantity $\Delta E(\lambda_4)$ (solid line **d**) as a function of λ_4 is shown in Fig. 2 together with the linear approximation (dashed line). The linear approximation is valid for $0 \leq \lambda_4 < 0.2$.

4.1.6 $\lambda_4 = \lambda_2 = 0$ composite model

The numerical results for the composite models with only one of the terms eq. (6-9) added to the $p = 1$ model show that there exist models with attractive or repulsive phases only. On the other hand, from the analysis of section 2.3.2 follows that for small coupling constants λ_A models with both attractive and repulsive phases can exist, provided at least one of the terms added to the $p = 1$ model leads to a repulsive phase and the other one leads to an attractive phase.

We studied numerically a model where the terms $\frac{5}{18 \times 32} \eta^{-4} \lambda_1 \mathcal{H}_1^{(2)}$ and $\frac{5}{18 \times 32} \eta^{-4} \lambda_3 \mathcal{H}_3^{(2)}$ are added to the $p = 1$ model. In Fig. 3a we show the energy *per unit topological charge* $E(\lambda_1, \lambda_3)/n$ for the charge-1 and charge-2 solutions as functions of λ_3 with $\lambda_1 = 0.01$ fixed. Both functions increase with λ_3 . For small values of λ_3 the energy *per unit topological charge* of the charge-2 solution (dashed-dotted line) is larger than the energy *per unit topological charge* of the charge-1 solution (solid line), whereas for larger values of λ_3 the energy *per unit topological charge* of the charge-1 solution is larger than the energy *per unit topological charge* of the charge-2 solution. The crossover occurs at $\lambda_3 \sim 0.22$ where both solutions have the same energy *per unit topological charge* $E/n \sim 1.085 \times 4\pi\eta$. Notice that attraction/repulsion occur for values of λ_3 above/below the crossover point, in contrast with the situation [10] in the Abelian Higgs model.

As expected, this model supports an attractive and an repulsive phase. The crossover is at a small value of the coupling constants λ_A and the energy *per unit topological charge* at this point is near the Bogolmol'nyi bound. However, in the example chosen the crossover is outside the range where the linear approximation is valid. From the linear approximation we can only predict the existence of attractive/repulsive phases, but not the features of the models in detail.

Another example is shown in Fig. 3b. Here the energy *per unit topological charge* is shown for the charge-1 solution (solid line) and the charge-2 solution (dashed-dotted line) as a function of λ_1 for fixed coupling constant $\lambda_3 = 1$. Again, for both solutions the energy *per unit topological charge* is an increasing function. There is an attractive phase for small values of λ_1 and a repulsive phase for large values of λ_1 . The crossover is at $\lambda_1 \sim 0.07$ where the energy *per unit topological charge* of both solutions is $E/n = 1.375 \times 4\pi\eta$. For large values of the coupling constant, like $\lambda_3 = 1$, the linear approximation is certainly not valid anymore. Still the model supports both an attractive and a repulsive phase. However, the energy *per unit topological charge* at the crossover now exceeds the Bogolmol'nyi bound considerably.

4.2 Composite model

In this section we consider the model defined by the Hamiltonian eq. (13), where the parts of the $p = 1$ model and the $p = 2$ model are treated on the same footing. The linear approximation of the energy *per unit topological charge* as a function of the coupling parameters λ_A is not applicable for this model.

As a typical example we discuss the charge-2 solution for the coupling constants $\lambda_A = 1$, $A = 1, \dots, 4$. The energies *per unit topological charge* of the charge-2 and charge-1 solutions are $E_{n=2}/2 = 2.1433 \times 4\pi\eta$ and $E_{n=1} = 2.05993 \times 4\pi\eta$, respectively. Thus the charge-2 solution is in the repulsive phase for these values of the coupling constants.

In Figs. 4a-4g we show the energy density and the field configuration for the charge-2 solution as functions of the dimensionless coordinates ρ and z . In Fig. 4a the energy density is shown. It possesses a maximum on the ρ -axis and it is monotonically decreasing along the z -axis, indicating a strong deviation from spherical symmetry. Like for the $p = 1$ model the surfaces of equal energy density form spheres and doughnuts.

Let us now compare the energy densities of the charge-2 solutions in the composite model and in the $p = 1$ model, shown in Fig. 1. At the origin the energy density of the composite model is roughly one order of magnitude larger than the energy density of the $p = 1$ model. In the composite model the energy density approaches its asymptotic value at a shorter distance from the origin than in the $p = 1$ model. Thus the composite model possesses a core with a high energy density, whereas the core in the $p = 1$ model is softer and more extended.

In Fig. 4b the gauge field function $H_1(\rho, z)$ is shown. According to the boundary conditions $H_1(\rho, z)$ vanishes on the ρ and z axis. It has a maximum located near the origin. For spherically symmetric solutions $H_1(\rho, z)$ would vanish identically. Thus $H_1(\rho, z)$ is excited due to the axial symmetry of the solution. Fig. 4c shows the gauge field function $H_2(\rho, z)$. The deviation from spherical symmetry for this function is small near the origin and nearly vanishing far away from the origin. The function $H_3(\rho, z)$ is exhibited in Fig. 4d. Similarly to the function $H_1(\rho, z)$ shown in Fig. 4b this function is excited due to the axial symmetry of the solution. Its maximum is located near the origin. Note that it is roughly one order of magnitude smaller than the maximum of the function $H_1(\rho, z)$. In Fig. 4e the function $H_4(\rho, z)$ is shown. Like the function $H_2(\rho, z)$ shown in Fig. 4.c the deviation from spherical symmetry is only small for this function. The Higgs field function $\phi_1(\rho, z)$ is shown in Fig. 4f. At the origin this function is linear in z for $\rho = 0$ whereas for $z = 0$ it is quadratic in ρ . For large distances from the origin the deviation from spherical symmetry almost vanishes. Fig. 4g shows the Higgs field function $\phi_2(\rho, z)$. It has a minimum near the origin and vanishes on the ρ and z axis due to the boundary conditions. Like the gauge field functions $H_1(\rho, z)$ and $H_3(\rho, z)$ this function is excited by the axial symmetry of the solution.

The gauge field functions and Higgs field functions possess a non-trivial dependence on the coordinates ρ and z only in the region near the origin where the core

of the energy density is located. As a result of our numerical integrations we have found that outside this core the functions decay to their vacuum values at infinity at a rate faster than a power behaviour. This is in contrast to the solutions of the $p = 1$ model, where in absence of the Higgs potential the Higgs fields possess a power law decay and only the gauge field functions decay exponentially. Thus for the composite model the asymptotic decay of the energy density outside the core originates not from the Higgs field functions but from the gauge field functions only.

Let us next look at the dependence of the energy on the coupling constants λ_A for the charge-1 and charge-2 solutions of the composite model.

We have solved numerically the partial differential equations for fixed $\lambda_4 = 1$ and several values of λ_A in the range $0 \leq \lambda_A \leq 1.5$ for $A = 1, 2, 3$. The results are exhibited in Fig. 5. Lines **a** and **a'** represent the energy *per unit topological charge* of the charge-1 and charge-2 solutions, respectively, as functions of the coupling constant λ_1 with $\lambda_2 = \lambda_3 = 1$ fixed. The lines cross at $\lambda_1 \sim 0.1$. Thus there is both an attractive phase ($\lambda_1 < 0.1$) and a repulsive phase ($\lambda_1 > 0.1$). The value of the energy *per unit topological charge* $E/n = 1.865 \times 4\pi\eta$ at the crossover is rather large compared to the Bolgolmol'nyi bound, which takes the value $1.1 \times 4\pi\eta$ for $\lambda_1 = 0.1$ in this case.

Lines **b** and **b'** represent the energy *per unit topological charge* of the charge-1 and charge-2 solutions, respectively, when λ_2 is varied with fixed $\lambda_1 = \lambda_3 = 1$. In the range $0 \leq \lambda_2 \leq 1.5$ the lines **b** and **b'** are almost parallel and there is no crossover. The upper lines correspond to the charge-2 solutions. There is a repulsive phase only in this case.

Finally we fix $\lambda_1 = \lambda_2 = 1$ and vary λ_3 . The energy *per unit topological charge* is represented in Fig. 5 by lines **c** and **c'** for the charge-1 and charge-2 solutions, respectively. Again, lines **c** and **c'** are almost parallel. Thus, there is only a repulsive phase.

4.3 $p = 2$ model

The numerical integration of the variational equations of the $p = 2$ model is a very difficult task. In the absence of the terms of the $p = 1$ model numerical instabilities arise leading to a failure of the algorithms. We succeeded to construct the spherically symmetric charge-1 solutions. However, we did not find the axially symmetric charge-2 solutions of the $p = 2$ model on its own. Instead we used an approximation procedure to calculate the energy of the charge-2 solutions as explained in the following.

We start with the composite model and regard now the $p = 1$ part as a perturbation. For that purpose we modify the static Hamiltonian eq. (13) by introducing the new coupling constant λ_0 ,

$$\hat{\mathcal{H}}^{(c)} = \lambda_0 \mathcal{H}^{(1)} + \eta^{-4} \mathcal{H}^{(2)}, \quad (49)$$

and consider the limit $\lambda_0 \rightarrow 0$. Assuming the existence of the solutions to the $p = 2$ model, we will now consider the model (49) as a perturbation of the latter by the

$p = 1$ model, characterised by a small value of the dimensionless coupling constant $\lambda_0 \ll 1$.

We expand the energy of the magnetic charge- n soliton in the vicinity of the parameter λ_0 ,

$$E^{(n)}(\lambda_0 + \Delta\lambda_0) = E^{(n)}(\lambda_0) + \Delta\lambda_0 \left. \frac{dE^{(n)}}{d\lambda_0} \right|_{\lambda_0} + o(\lambda_0^2). \quad (50)$$

With the same reasoning as in section 2.3.2, the quantity $\left. \frac{dE^{(n)}}{d\lambda_0} \right|_{\lambda_0=0}$ can be calculated exclusively in terms of the exact solutions. Now, because we assumed that λ_0 is very small, we can evaluate (50) at $\Delta\lambda_0 = -\lambda_0$. Thus for sufficiently small λ_0 ,

$$E^{(n)}(0) \approx E^{(n)}(\lambda_0) - \lambda_0 \left. \frac{dE^{(n)}}{d\lambda_0} \right|_{\lambda_0} \quad (51)$$

will give a very good approximation to the energy of a solution of the $p = 2$ model. This energy consists of two terms, the first is the energy of the modified $p = 2$ model for a small value of λ_0 . The second term is given by $-\lambda_0 \int \mathcal{H}^{(1)} d^3r$ evaluated for the solution with finite (but small) λ_0 .

We can now estimate the energy of the $p = 2$ model on its own by calculating the energy of the modified composite model for a very small value of λ_0 and by subtracting the contribution of the $p = 1$ part, i. e. the quantity $\lambda_0 \int \mathcal{H}^{(1)} d^3r$ evaluated with the solution for the small value of λ_0 .

To check the validity of our limiting scheme, we followed this procedure for a set of decreasing values of λ_0 and found, that the estimated energy becomes indeed a constant for λ_0 small enough.

Let us first we discuss the properties of charge-2 solutions for the $p = 2$ model at the *critical* values of the coupling constants $\lambda_A = 1$, $A = 1, \dots, 4$, determined by the investigation of the charge-1 solutions. The energy *per unit topological charge* of the charge-1 solution was found to be $E^{(1)}(\lambda_A = 1) = 1.0002 \times 4\pi\eta$, whereas for the charge-2 solutions we find for the same coupling constants $E^{(2)}(\lambda_A = 1)/2 = 1.003 \times 4\pi\eta$. Thus the like monopoles repel for the *critical* values of the coupling constants. If we compare with the Bogolmol'nyi bound, given by $4\pi\eta$, we see that for both the charge-1 and charge-2 solutions the energies *per unit topological charge* are very close to the lower bound, indeed.

In order to compare the $p = 2$ model with the $p = 1$ model and the composite model we show in Fig. 6a-6g the energy density, the gauge field functions and the Higgs field functions for the solution of the modified model (49) for the coupling constants $\lambda_0 = 0.01$, $\lambda_A = 1$, $A = 1, \dots, 4$ and assume that this configuration is close to the solution of the $p = 2$ model on its own.

The energy density, shown in Fig. 7a as a function of the dimensionless coordinates ρ and z , is similar to the energy density of the composite model, shown in Fig. 4a. It possesses a maximum on the ρ -axis near the origin and it is monotonically decreasing along the z -axis. Its value at the origin is of the same magnitude as for the composite

model and the decay for large distances from the origin is slightly faster. Like for the $p = 1$ model and the composite model the surfaces of equal energy density form spheres und doughnuts.

The gauge field functions and the Higgs field functions are shown in Figs. 6b-6e and Figs. 6f-6g, respectively. They look very simmilar to the solution of the composite model shown in Figs. 4b-g, except for the gauge field function $H_3(\rho, z)$. For the $p = 2$ model $H_3(\rho, z)$ is negative and its minimum is of the order ≈ -0.1 , whereas for the composite model it is positive with a maximum of the order ≈ 0.025 .

Let us next look at the dependence of the energy on the coupling constants λ_A for the charge-1 and charge-2 solutions. For the $p = 2$ model we have fixed the coupling constant $\lambda_4 = 1$. For the charge-1 solutions we solved the ordinary differential equations of the $p = 2$ model for several values of the coupling constants. The energy for the charge-2 solutions are calculated approximately as discussed above.

The results are shown in Fig. 7a-7c. In Fig. 7a we exhibit the energy *per topological charge* of the charge-1 solution (solid line) and the charge-2 solution (dashed-dotted line) as a function of the coupling constant λ_1 with fixed $\lambda_2 = \lambda_3 = 1$. Both lines cross at $\lambda_1 = 0.89$. There is an attractive phase for $\lambda_1 < 0.89$ and a repulsive phase for $\lambda_1 > 0.89$. The energy *per topological charge* at the crossing is $E/n = 0.9898 \times 4\pi\eta$. As expected the crossover takes place at values of the coupling constants near the *critical* values $\lambda_1 = \lambda_2 = \lambda_3 = 1$.

In Fig. 7b we exhibit the energy *per topological charge* of the charge-1 solution (solid line) and the charge-2 solution (dashed-dotted line) as a function of the coupling constant λ_2 with fixed $\lambda_1 = \lambda_3 = 1$. In this case the crossing is at $\lambda_2 = 1.07$, with a repulsive phase for $\lambda_2 < 1.07$ and an attractive phase for $\lambda_2 > 1.07$. For the energy *per topological charge* at the crossing the value $E/n = 1.0333 \times 4\pi\eta$ was found. Again, the values of the coupling constants at the crossing are near the *critical* values.

In Fig. 7c we exhibit the energy *per topological charge* of the charge-1 solution (solid line) and the charge-2 solution (dashed-dotted line) as a function of the coupling constant λ_3 with fixed $\lambda_1 = \lambda_2 = 1$. In this case the crossing occurs for a value of the coupling constants $\lambda_3 = 1.49$, which is considerably larger then the *critical* value $\lambda_3 = 1$. There is a repulsive phase for $\lambda_3 < 1.49$ and an attractiv phase for $\lambda_3 > 1.49$. The energy *per topological charge* at the crossing takes the value $E/n = 1.1969 \times 4\pi\eta$.

Notice that the situation in Figs. 7b and 7c, namely that of attraction/repulsion taking place for values of the coupling constants larger/smaller than that of the crossover point, contrasts with the corresponding situation [10] for the Abelian Higgs model.

5 Summary and Conclusions

The main aim of the present paper was to acheive monopole field configurations in which like-monopoles can attract as well as repel. We found this to be the case in various new 3 dimensional $SO(3)$ gauged Higgs models with isovector Higgs fields. Such a property contrasts with the 't Hooft-Polyakov monopoles of the Georgi-Glashow

model, in which like-monopoles only repel. The main model we employed was one we described as the $p = 2$ model because it is the second one in a hierarchy of models descended from $4p$ dimensional YM systems [13], the first one of which, $p = 1$, is the GG model in the PS limit. The spherically symmetric magnetic charge-1 solutions of the $p = 2$ model were previously studied, from which we concluded that the type of behaviour sought in the present work was likely to materialise. Accordingly in the present investigation, we studied the charge-2 axially symmetric solutions of this model, and found indeed that for some values of the dimensionless coupling parameters the interaction energies of the monopoles led to bound states. In this sense, the 3 dimensional $p = 2$ model is very similar to the 2 dimensional Abelian Higgs model, both featuring a crossover between an attractive and a repulsive phase. Indeed, our procedures were the same employed by Jacobs and Rebbi [10] in the 2 dimensional case. There is however, a qualitative difference between these models in the sense that the attractive and repulsive phases of the $p = 2$ model occur on the opposite sides of the crossover points for some of the coupling constants. Another difference between these models is that in the $p = 2$ case there is really no genuinely non-interacting, minimal, field configuration. Nevertheless there is an almost non-interacting field configuration which was discussed in some detail in [15], which turns out to be approximately the crossover point between the two phases.

In addition to the $p = 2$ model, we studied combinations of the $p = 1$, and the $p = 2$ models, as well as extensions of the $p = 1$ model by some of the constituent terms in the $p = 2$ model which is tantamount to adding a particular Skyrme-like term. In some of the latter examples we also considered small perturbations of the $p = 1$ model, something which is radically different from adding the Higgs potential to the $p = 1$ model to obtain the GG model. (Recall that the BPS solutions cannot be related to the monopoles of the GG model perturbatively.) Perhaps the most interesting outcome of the latter considerations was the construction of extended $p = 1$ models whose monopole solutions feature either an attractive phase only or a repulsive phase only, between two like-monopoles.

Apart from their intrinsic interest in providing generalised monopoles exhibiting both attractive and repulsive phases, it is hoped that this property of the generalised monopoles may be of some potential interest in the role of monopoles in grand unified theory, and possibly to the cosmic monopole problem [23]. The models we have considered could occur as extensions of the usual models of the grand unified theory. In such models there is attraction between like-monopoles (and ofcourse like-antimonopoles) as happens with type I cosmic strings [24]. We do not speculate here on the possible consequences of this analogy. Perhaps the most likely effect of such (generalised) monopoles may occur in the gravitational clumping [25] of monopoles leading to the annihilation of monopole-antimonopole pairs. In contrast with the usual theory, there will be only attractive forces between the monopoles, independently of the gravitational interaction.

Acknowledgements This work was supported by Basic Science SC/96/636 and SC/95/602 grants of Forbairt.

References

- [1] G. 't Hooft, Nucl. Phys. **B 79** (1974) 276.
- [2] A.M. Polyakov, JETP Lett. **20** (1974) 194.
- [3] M.K. Prasad and C.M. Sommerfield, Phys. Rev. Lett. **35** (1975) 760.
- [4] see A. Jaffe and C. J. Taubes, Monopoles and Vortices, Birkhäuser, Basel, 1980.
- [5] N. S. Manton, Nucl. Phys. **B 126** (1977) 525.
- [6] W. Nahm, Phys. Lett. **B 79** (1978) 426; *ibid.* **B 85** (1979) 373.
- [7] J. N. Goldberg, P. S. Jang, S. Y. Park and K. C. Wali, Phys. Rev. **D 18** 542 (1978).
- [8] V. G. Kiselev and Ya. M. Shnir, "Interaction of non-Abelian monopole with external field", hep-th/9702033.
- [9] B. Kleihaus, J. Kunz and D.H. Tchrakian, "Interaction energy of 't Hooft-Polyakov monopoles", hep-th/9804192.
- [10] L. Jacobs and C. Rebbi, Phys. Rev. **B 19** (1979) 4486.
- [11] K. Arthur, Y. Brihaye and D.H. Tchrakian, "Interaction Energy of Generalised Abelian Higgs Vortices", to appear in J. Math. Phys.
- [12] C. Rebbi and P. Rossi, Phys. Rev. **D 22** (1980) 2010.
- [13] D.H. Tchrakian, J. Math. Phys, **21** (1980) 166 ; Phys. Lett. **B 150** (1985) 360; Int. J. Mod. Phys. A (Proc. Suppl.) **3A** (1993) 584.
- [14] D.H. Tchrakian and A. Chakrabarti, J. Math. Phys. **32** (1991) 2532.
- [15] B. Kleihaus, D. O'Keeffe and D.H. Tchrakian, "Calculation of the mass of a generalised monopole", Phys. Lett **B** (to appear).
- [16] D.H. Tchrakian, "Skyrme-like models in gauge theory", in Constraint theory and quantisation methods, eds. F. Colomo, L. Lusanna and G. Marmo, World Scientific, 1994.
- [17] T.H.R. Skyrme, Proc. Roy. Soc. **A 260** (1961) 127; Nucl. Phys. **31** (1962) 556.
- [18] E.B. Bogomol'nyi, Sov. J. Nucl. Phys. **24** (1976) 449.
- [19] N.S. Manton, Nucl. Phys. **B 135** (1978) 319.
- [20] B. Kleihaus, J. Kunz and Y. Brihaye, Phys. Lett. **B273** (1991) 104; J. Kunz, B. Kleihaus and Y. Brihaye, Phys. Rev. D **46** (1992) 3587; Y. Brihaye, B. Kleihaus and J. Kunz, Phys. Rev. D **47** (1993) 1664; B. Kleihaus and J. Kunz, Phys. Lett. **B329** (1994) 61; Phys. Rev. D **50** (1994) 5343.
- [21] Y. Brihaye and J. Kunz, Phys. Rev. D **50** (1994) 4175.

- [22] W. Schönauer and R. Weiß, J. Comput. Appl. Math. 27, (1989) 279; M. Schauder, R. Weiß and W. Schönauer, The CADSOL Programm Package, Universität Karlsruhe, Interner Bericht Nr. 66/92 (1992).
- [23] T.W.B. Kibble, Trieste 1981
- [24] T.W.B. Kibble, Phys. Rep. **69** (1980) 183.
- [25] T. Glodman, E. W. Kolb and D. Toussaint, Phys. Rev. D **23** (1981) 867.

Figure captions

Fig. 1

The energy density in units of η^4 of the $p = 1$ model is shown as a function of the dimensionless coordinates $\rho = \eta r \sin \theta$ and $z = \eta r \cos \theta$.

Fig. 2

The quantity $\Delta E(\lambda_A) = E^{(2)}(\lambda_A)/2 - E^{(1)}(\lambda_A)$ in units of $4\pi\eta$ (solid lines) is shown as a function of λ_A with $\lambda_B = 0$, $B \neq A$. The dash-dotted lines indicate the slope at $\lambda_A = 0$. Line **a** corresponds to $\lambda_1 \neq 0$, line **b** to $\lambda_2 \neq 0$, line **c** to $\lambda_3 \neq 0$ and line **d** to $\lambda_4 \neq 0$, respectively.

Fig. 3a

The energy *per unit topological charge* in units of $4\pi\eta$ is shown as a function of λ_3 with $\lambda_1 = 0.01$, $\lambda_2 = \lambda_4 = 0$ for the charge $n = 1$ solution (solid line) and for the charge $n = 2$ solution (dash-dotted line).

Fig. 3b

The same as Fig. 3a for λ_1 with $\lambda_3 = 1$ and $\lambda_2 = \lambda_4 = 0$.

Fig. 4a

The energy density in units of η^4 of the charge $n = 2$ solution of the composite model with $\lambda_A = 1$, $A = 1, \dots, 4$ is shown as a function of the dimensionless coordinates $\rho = \eta r \sin \theta$ and $z = \eta r \cos \theta$.

Fig. 4b

The same as Fig. 4a for the gauge field function $H_1(\rho, z)$.

Fig. 4c

The same as Fig. 4a for the gauge field function $H_2(\rho, z)$.

Fig. 4d

The same as Fig. 4a for the gauge field function $H_3(\rho, z)$.

Fig. 4e

The same as Fig. 4a for the gauge field function $H_4(\rho, z)$.

Fig. 4f

The same as Fig. 4a for the Higgs field function $\phi_1(\rho, z)$.

Fig. 4g

The same as Fig. 4a for the Higgs field function $\phi_2(\rho, z)$.

Fig. 5

The energy *per unit topological charge* in units of $4\pi\eta$ of the composite model is shown as a function of λ_A , $A = 1, 2, 3$ with fixed $\lambda_B = 1$, $B \neq A$ for the charge $n = 1$ solutions

(solid lines) and for the charge $n = 2$ solutions (dash-dotted lines). Lines **a** and **a'** correspond to $\lambda_2 = \lambda_3 = \lambda_4 = 1$, lines **b** and **b'** to $\lambda_1 = \lambda_3 = \lambda_4 = 1$, and lines **c** and **c'** to $\lambda_1 = \lambda_2 = \lambda_4 = 1$, respectively. The thin solid line indicates the Bogolmol'nyi bound.

Fig. 6a

The energy density in units of η^4 of the charge $n = 2$ solution of the $p = 2$ model with $\lambda_A = 1$, $A = 1, \dots, 4$ is shown as a function of the dimensionless coordinates $\rho = \eta r \sin \theta$ and $z = \eta r \cos \theta$.

Fig. 6b

The same as Fig. 6a for the gauge field function $H_1(\rho, z)$.

Fig. 6c

The same as Fig. 6a for the gauge field function $H_2(\rho, z)$.

Fig. 6d

The same as Fig. 6a for the gauge field function $H_3(\rho, z)$.

Fig. 6e

The same as Fig. 6a for the gauge field function $H_4(\rho, z)$.

Fig. 6f

The same as Fig. 6a for the Higgs field function $\phi_1(\rho, z)$.

Fig. 6g

The same as Fig. 6a for the Higgs field function $\phi_2(\rho, z)$.

Fig. 7a

The energy *per unit topological charge* in units of $4\pi\eta$ of the $p = 2$ model is shown as a function of λ_1 with fixed $\lambda_A = 1$, $A \neq 1$ for the charge $n = 1$ solution (solid line) and for the charge $n = 2$ solution (dash-dotted Line). The thin solid line indicate the topological bound.

Fig. 7b

The same as Fig. 7a for λ_2 with fixed $\lambda_A = 1$, $A \neq 2$.

Fig. 7c

The same as Fig. 7a for λ_3 with fixed $\lambda_A = 1$, $A \neq 3$.

	$1/n \left. dE/d\lambda_A \right _{\lambda_A=0}$		c_A
A	$n = 1$	$n = 2$	
1	0.688	2.925	2.237
2	0.383	0.437	0.054
3	0.367	0.291	-0.076
4	0.061	0.020	-0.041

Table 1

The quantity $\frac{1}{n} \left. \frac{dE^{(n)}}{d\lambda_A} \right|_{\lambda_A=0}$ defined in (19) for the Hamiltonians $\mathcal{H}_A^{(2)}$ is given for the charge-1 and charge-2 solutions together with their difference c_A in units of $4\pi\eta$.

Fig. 1

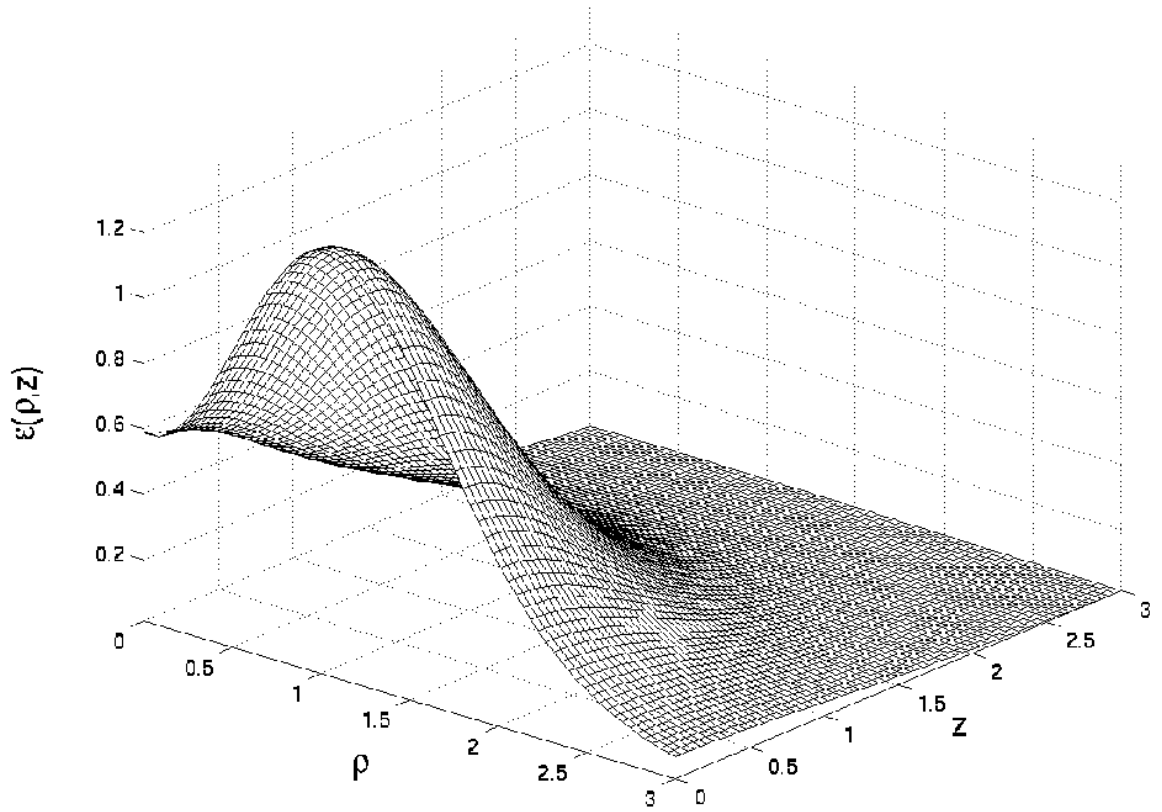


Fig. 2

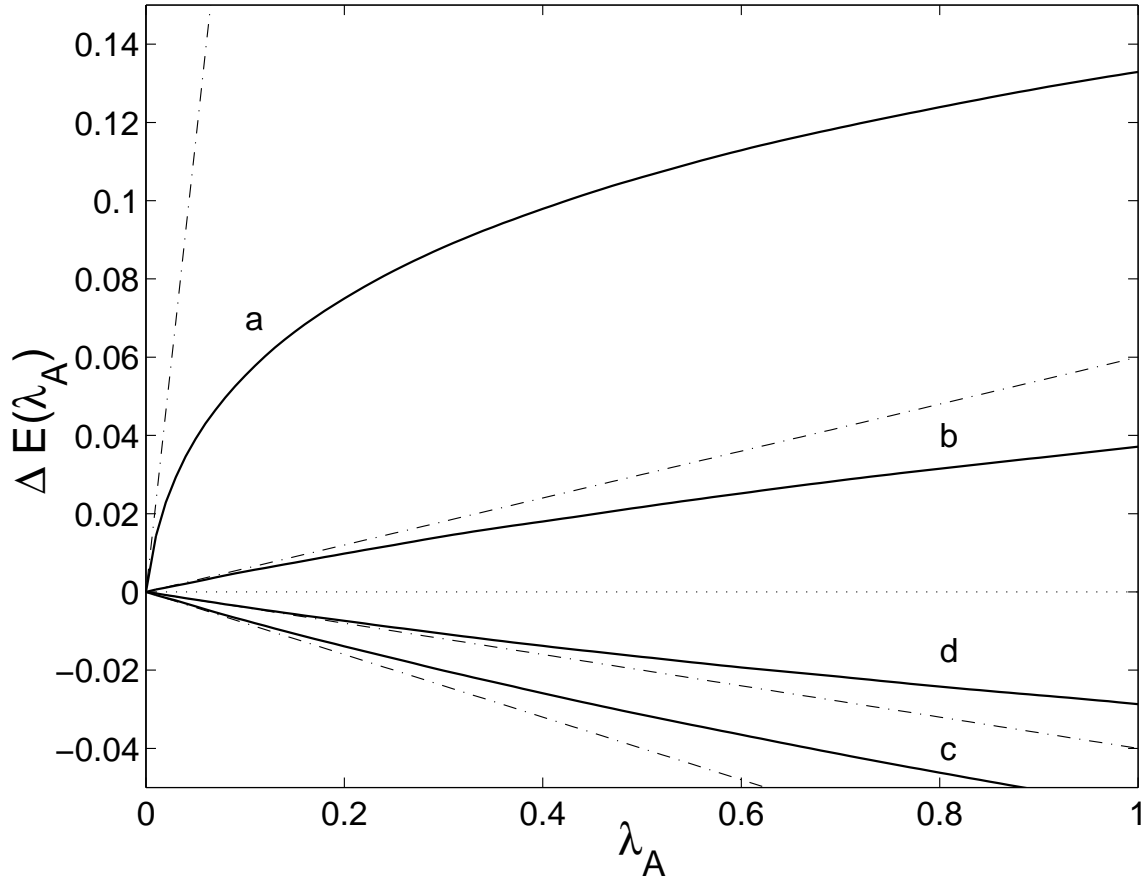


Fig. 3a

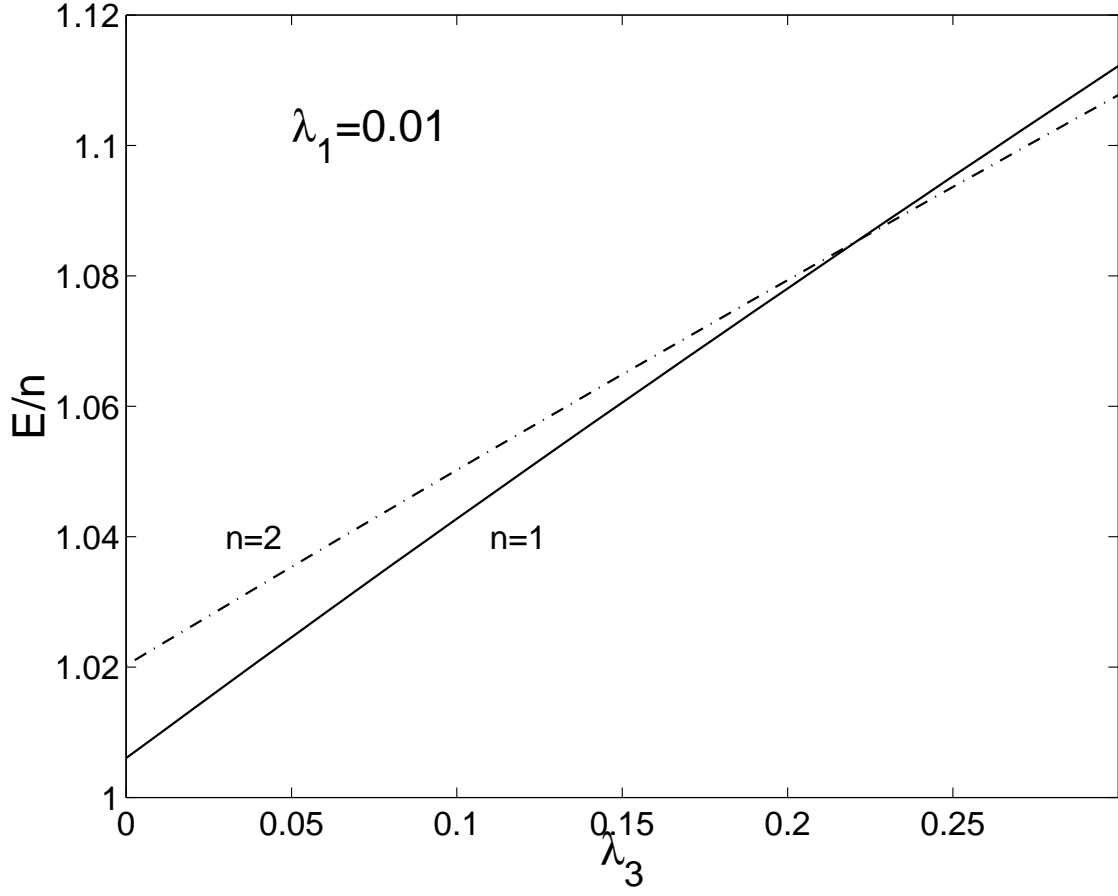


Fig. 3b

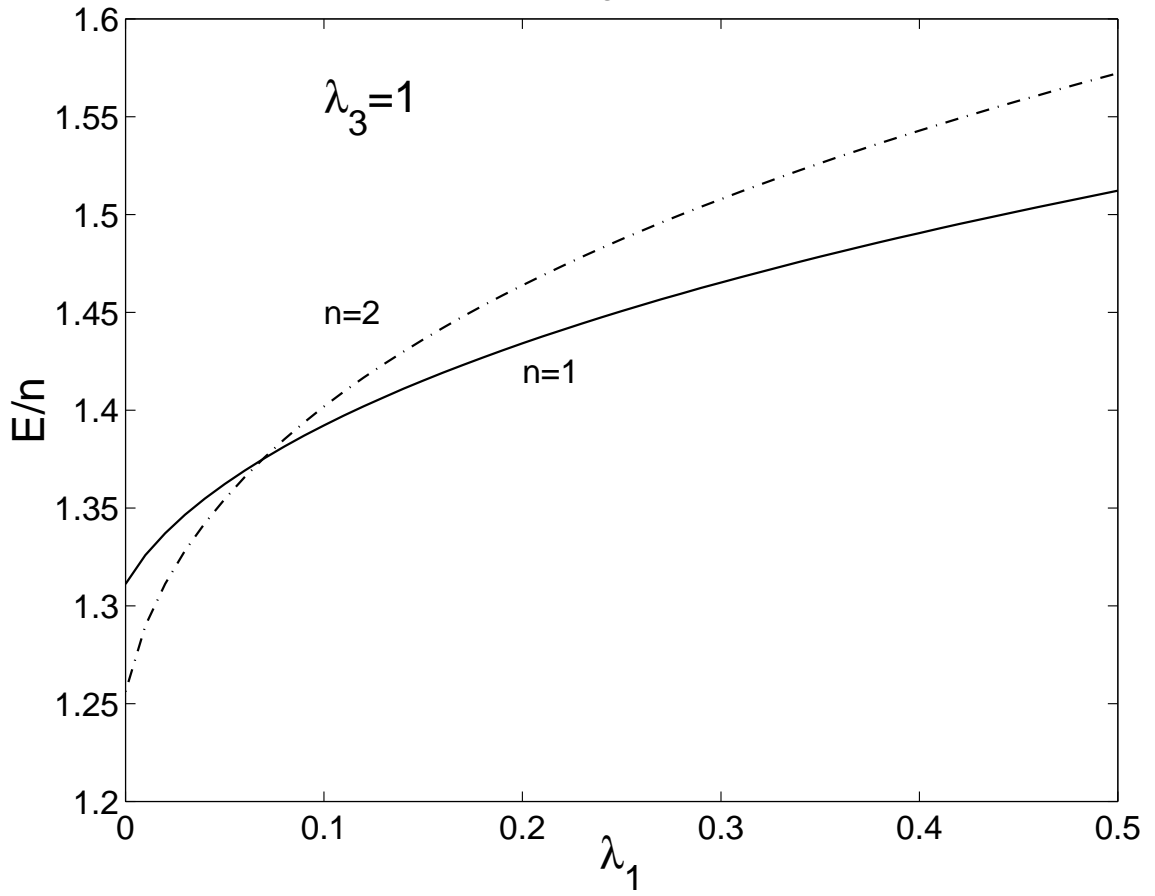


Fig. 4a

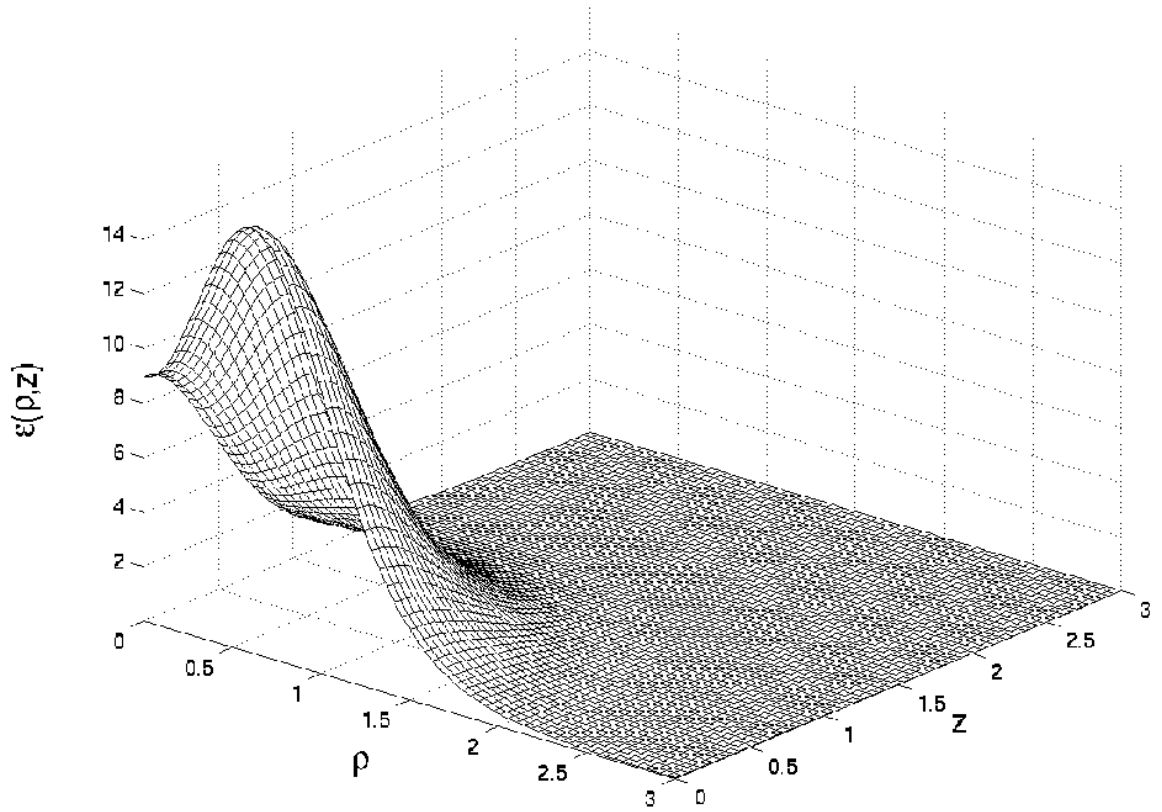


Fig. 4b

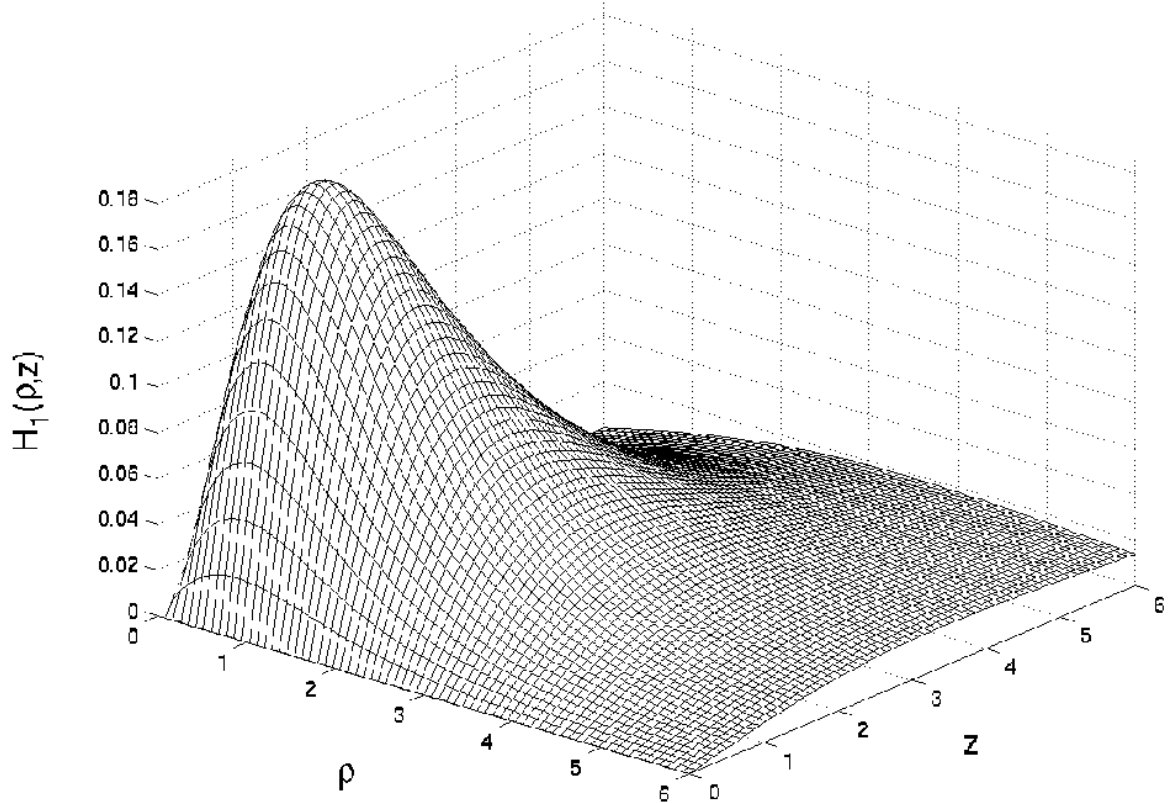


Fig. 4c

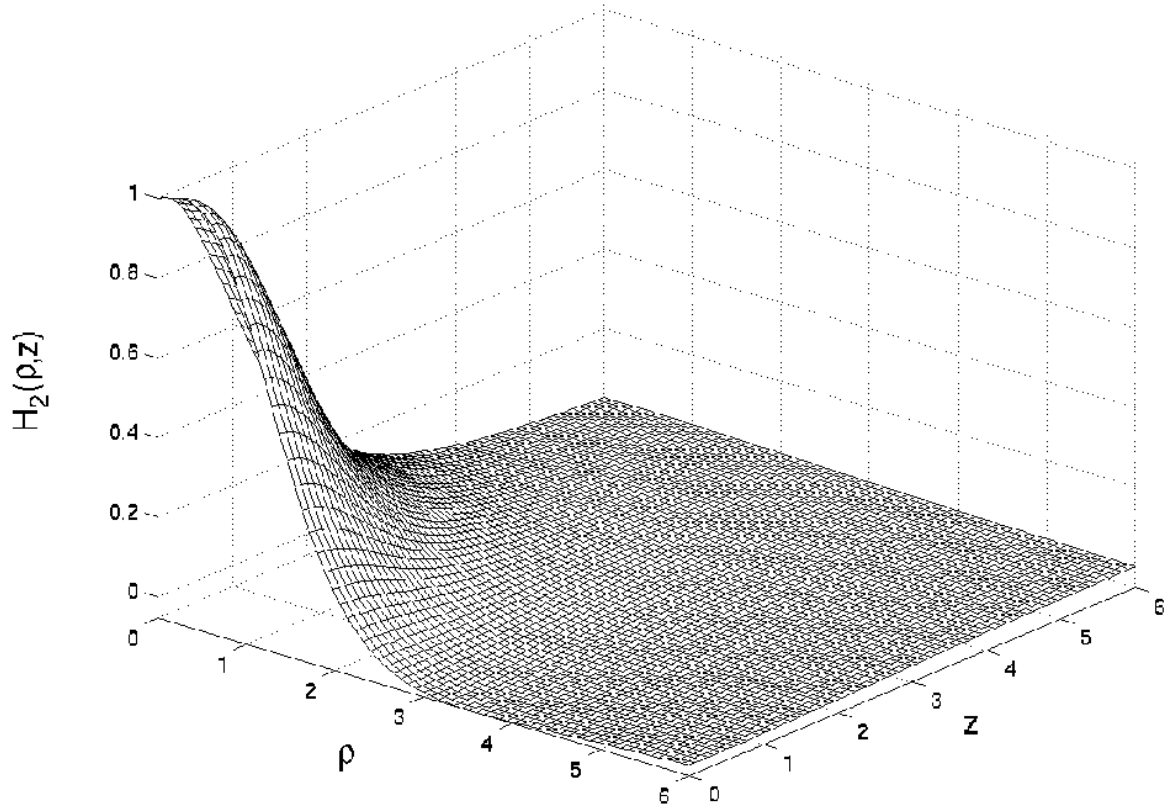


Fig. 4d

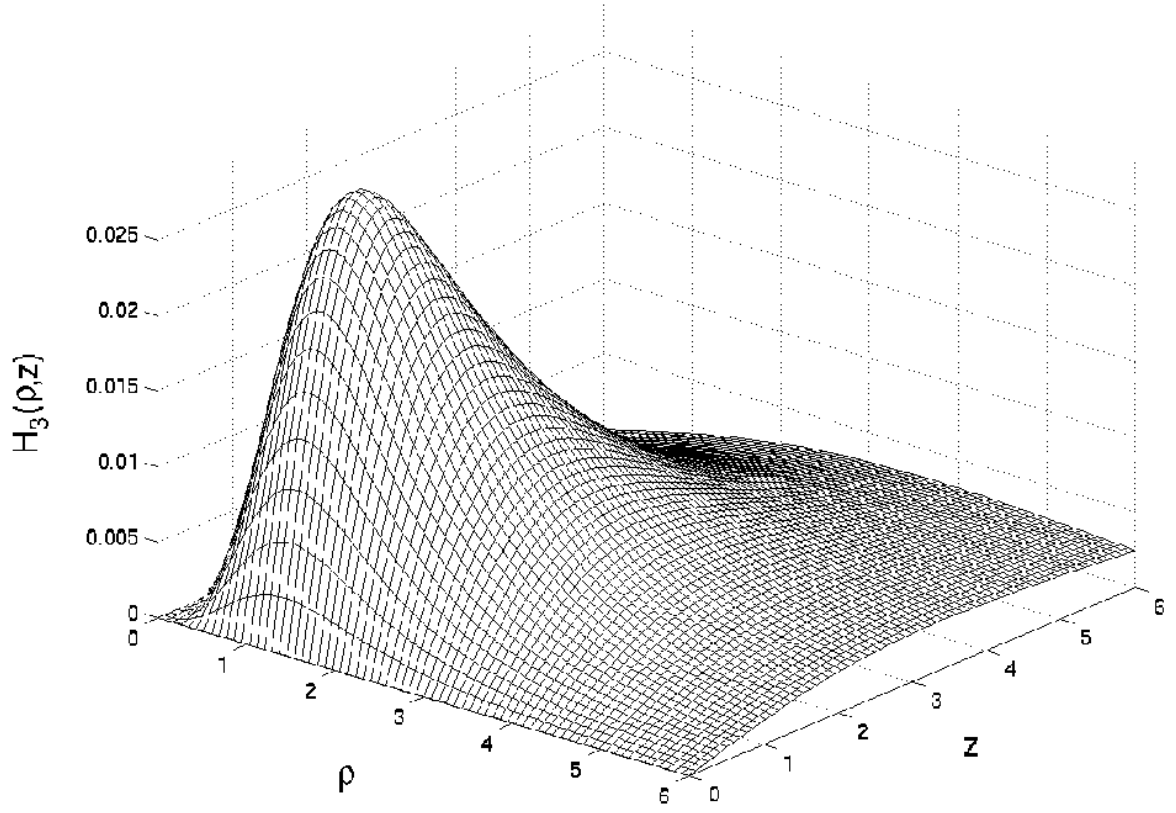


Fig. 4e

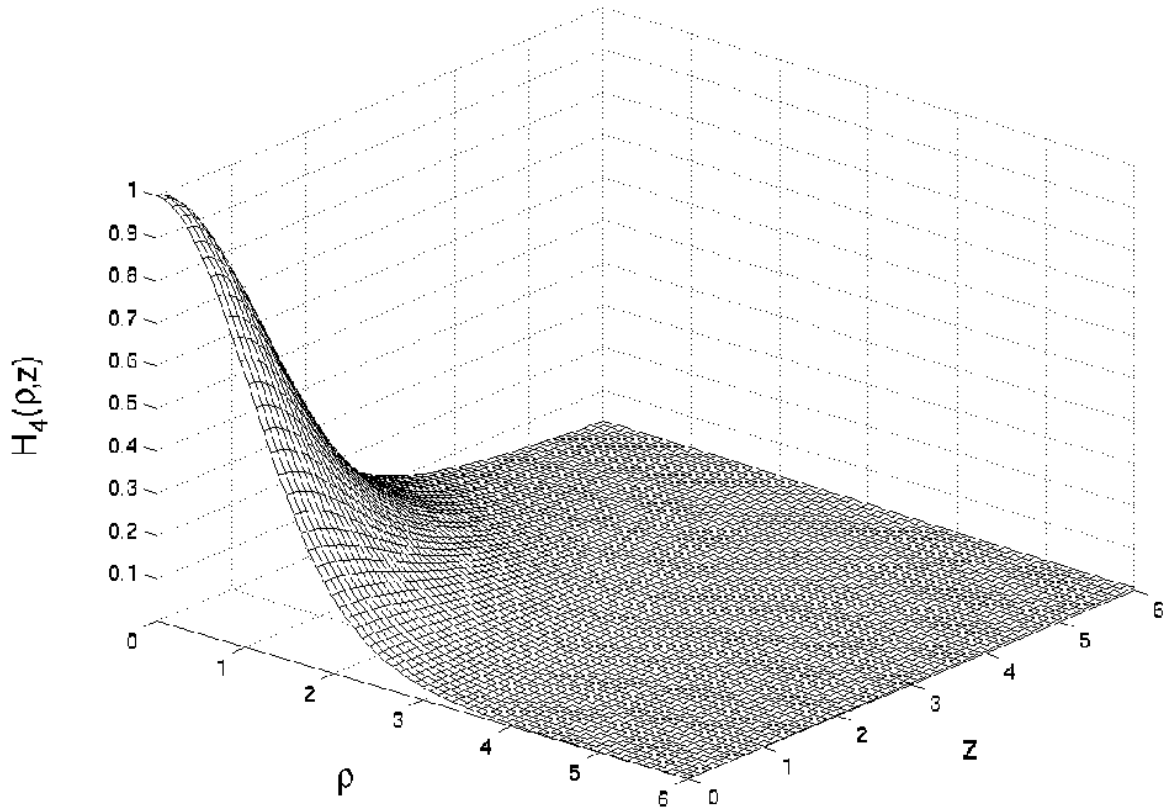


Fig. 4f

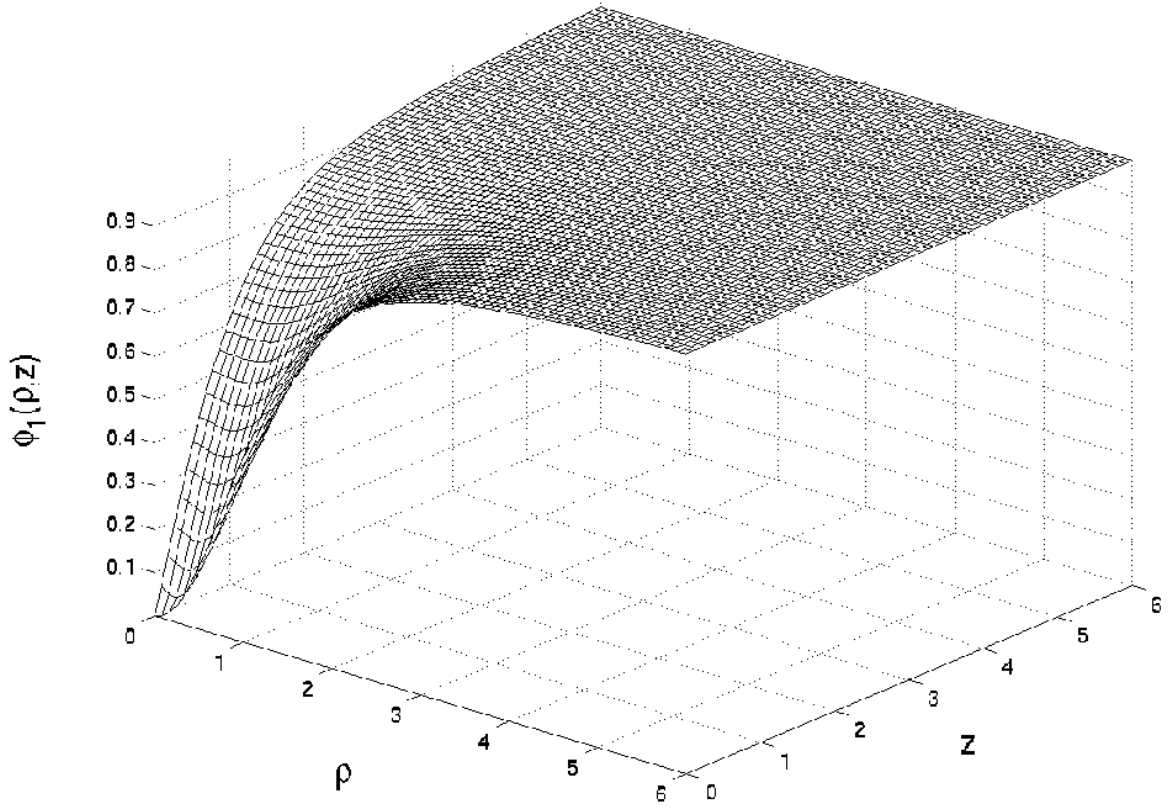


Fig. 4g

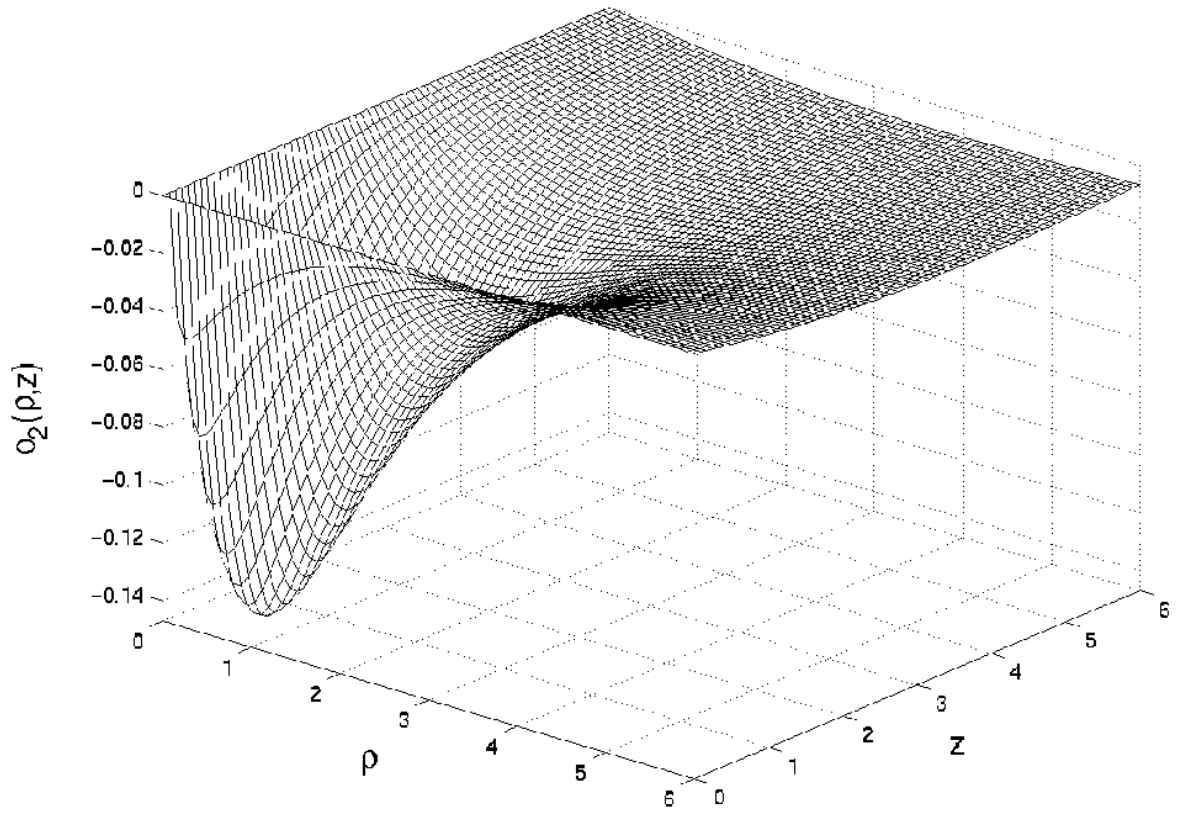


Fig. 5

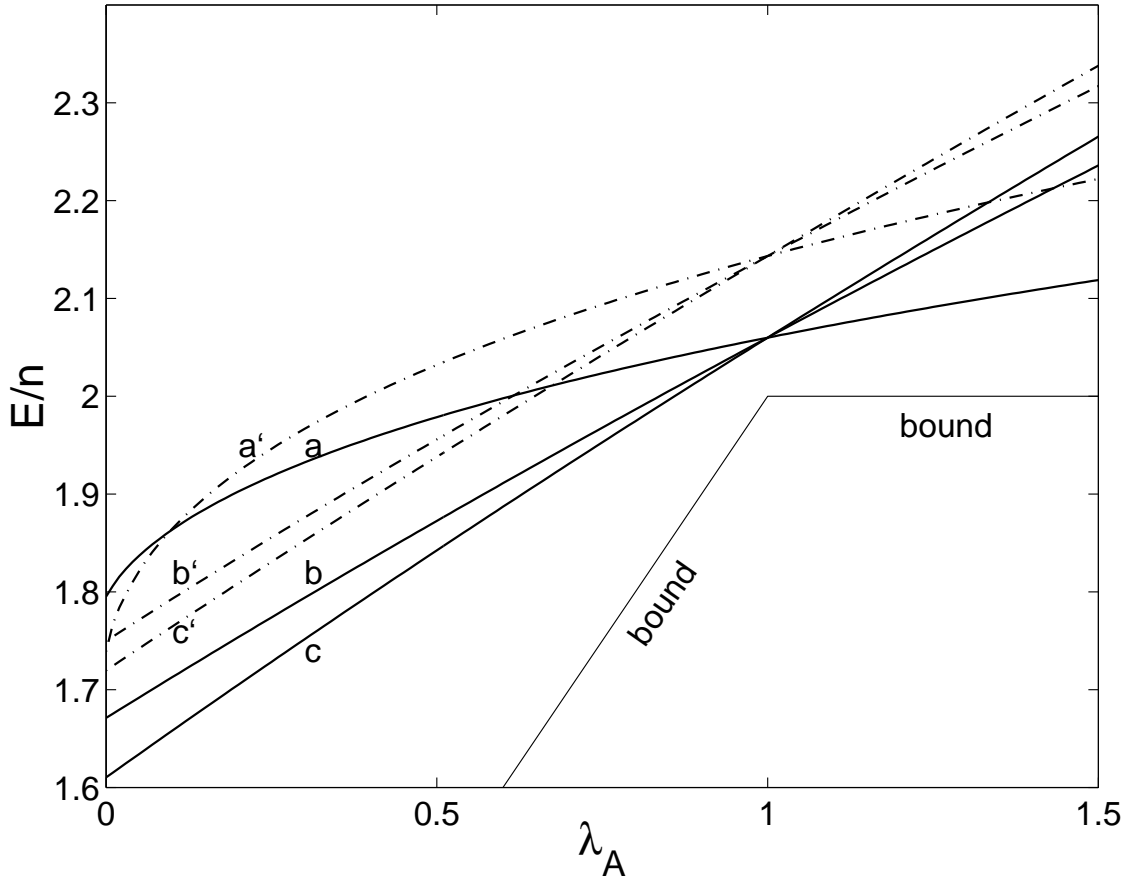


Fig. 6a

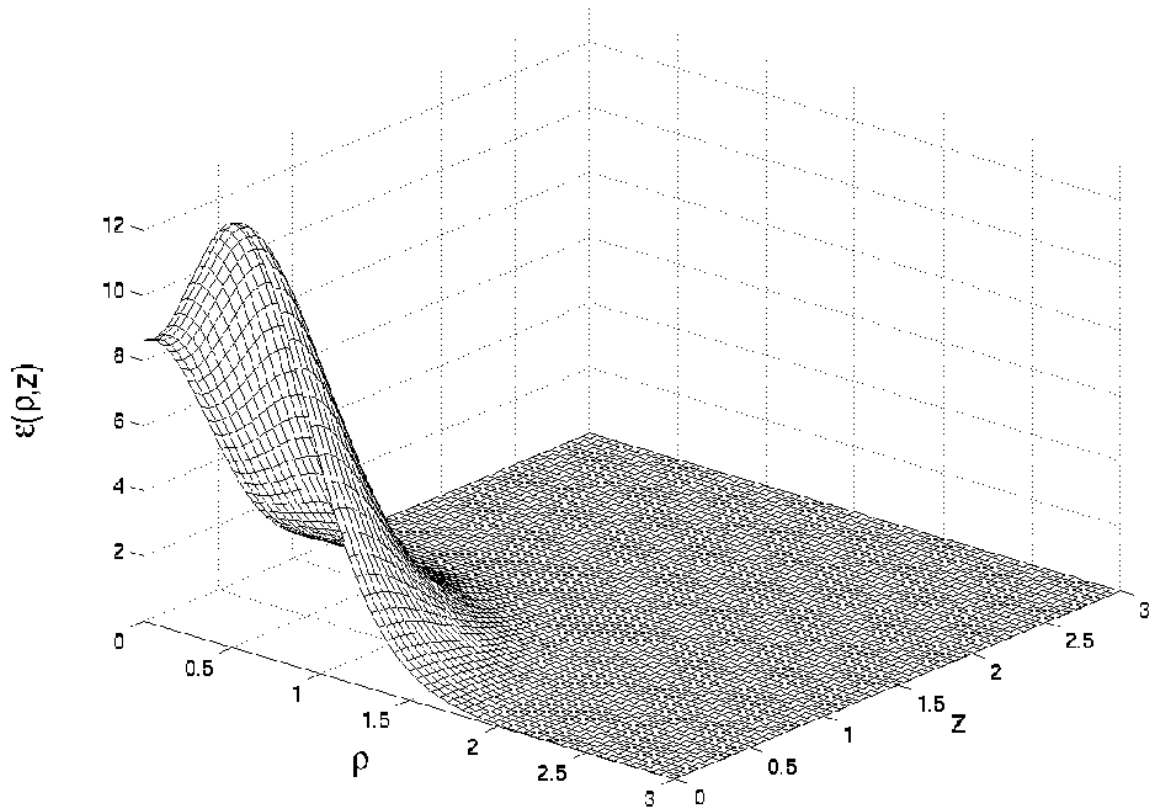


Fig. 6b

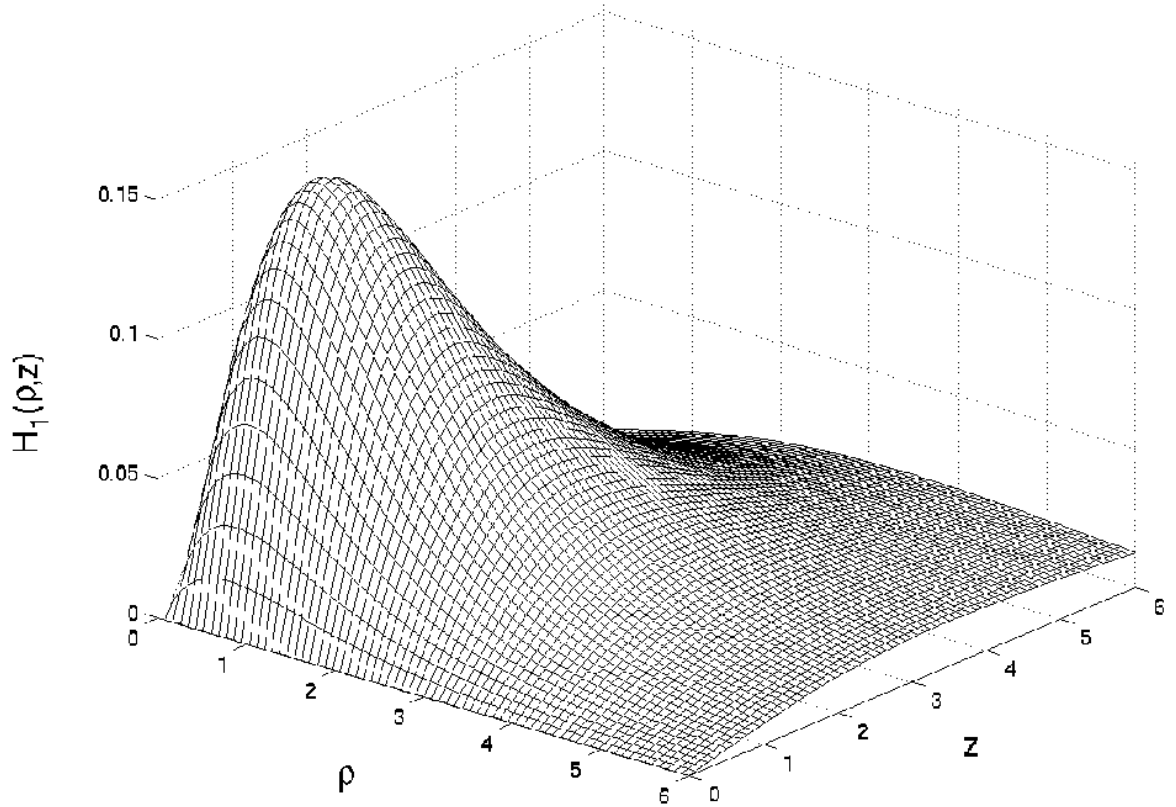


Fig. 6c

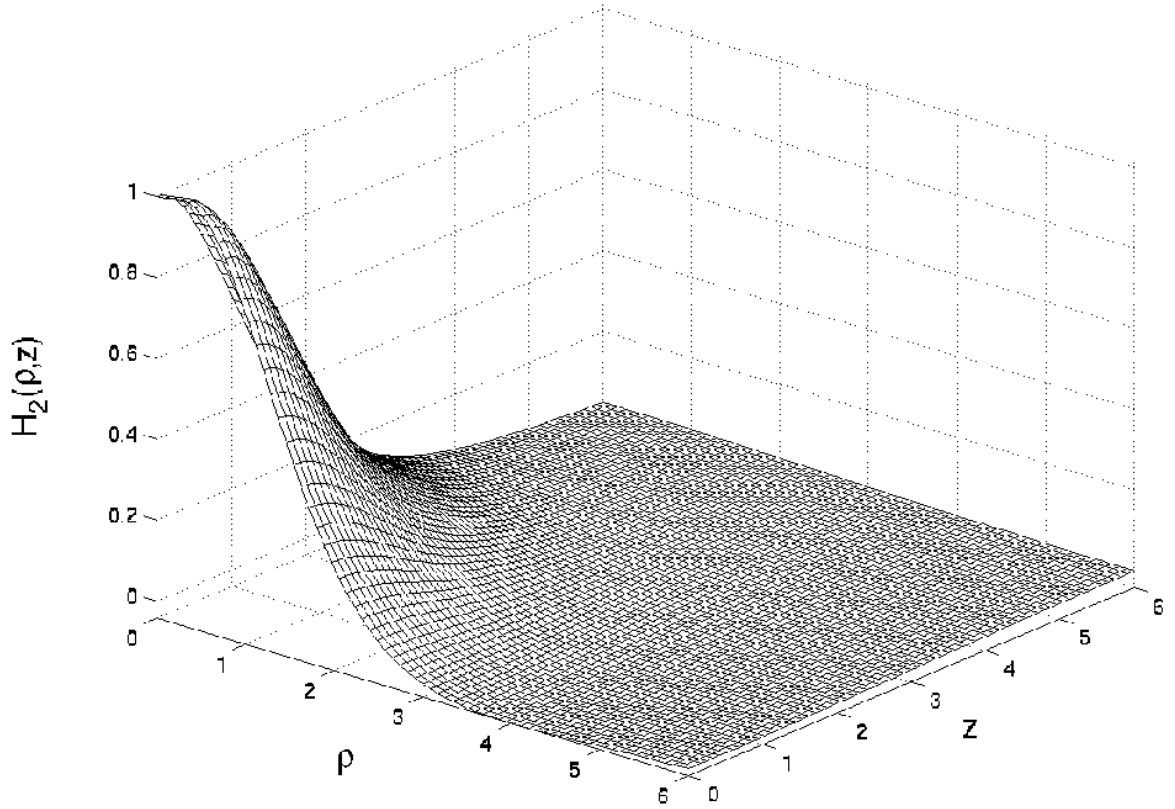


Fig. 6d

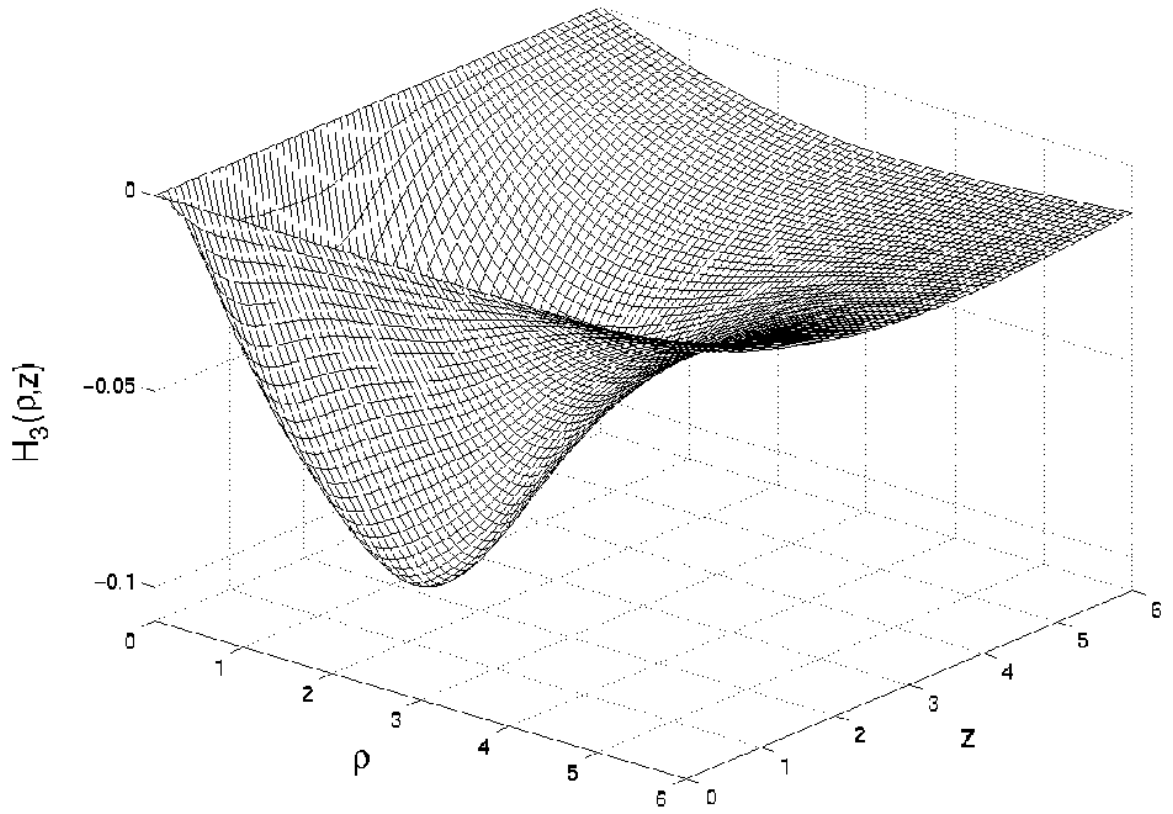


Fig. 6e

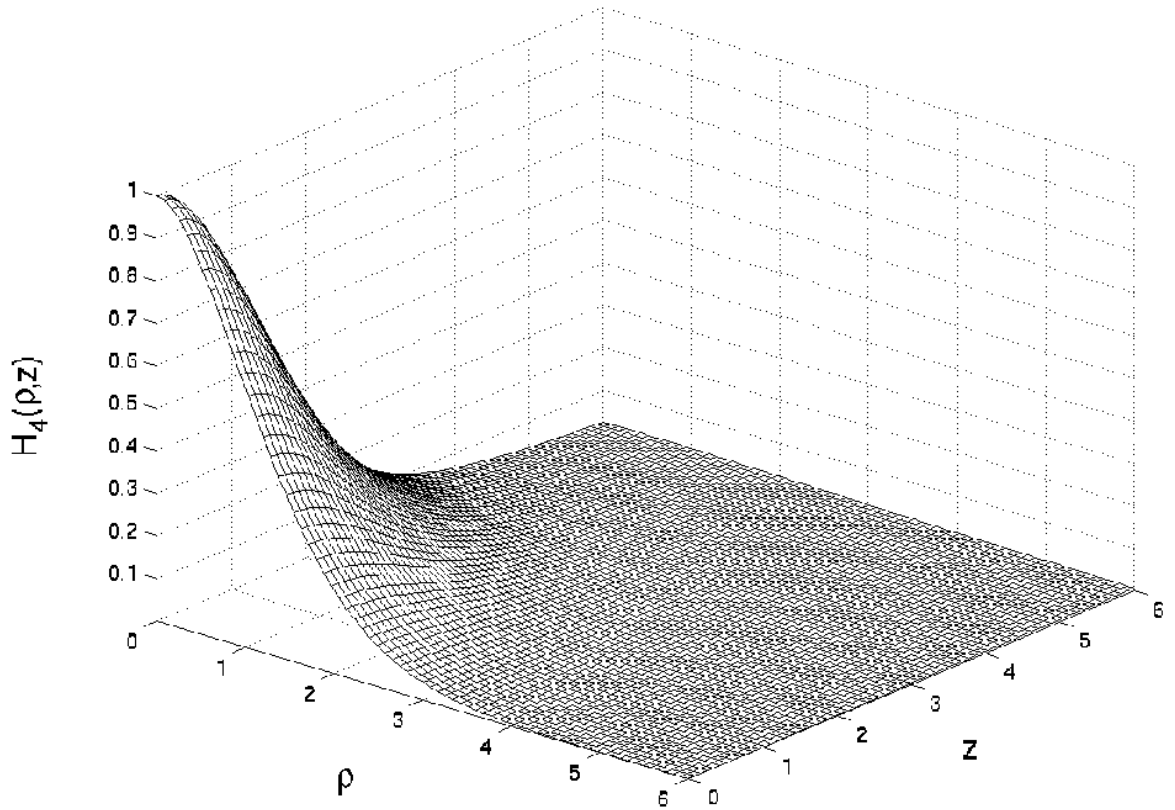


Fig. 6f

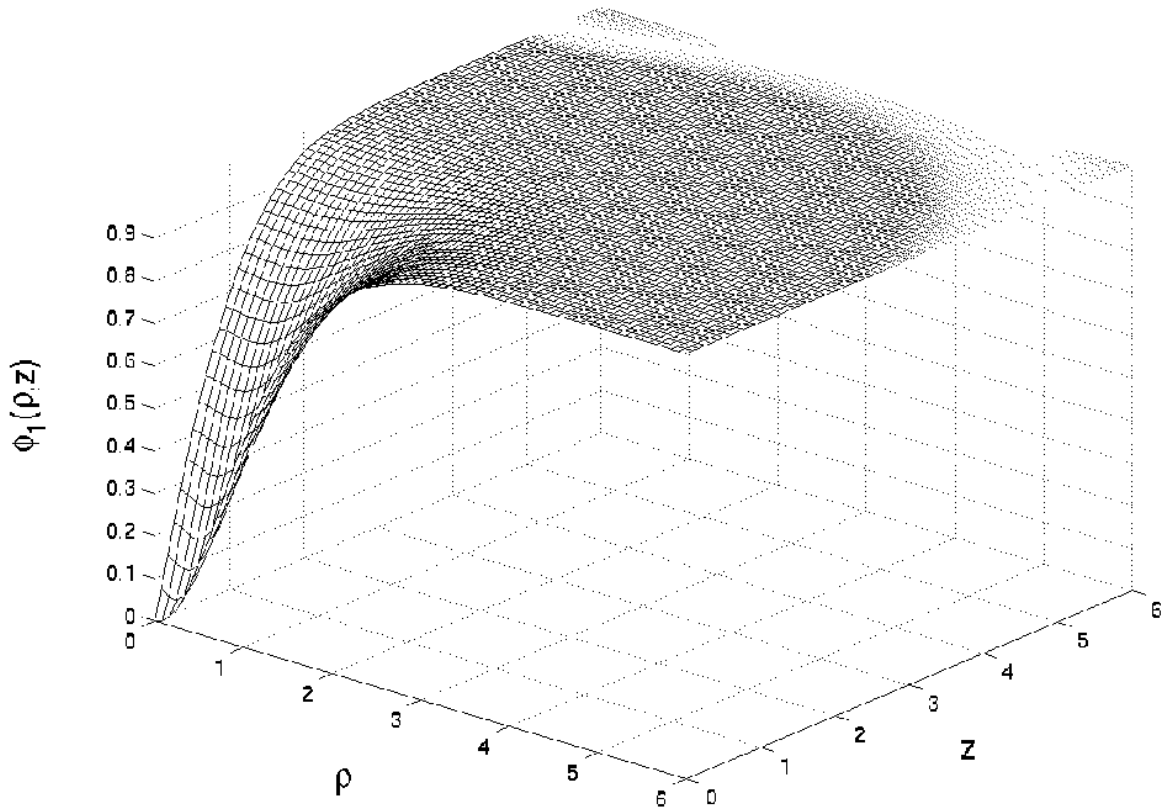


Fig. 6g

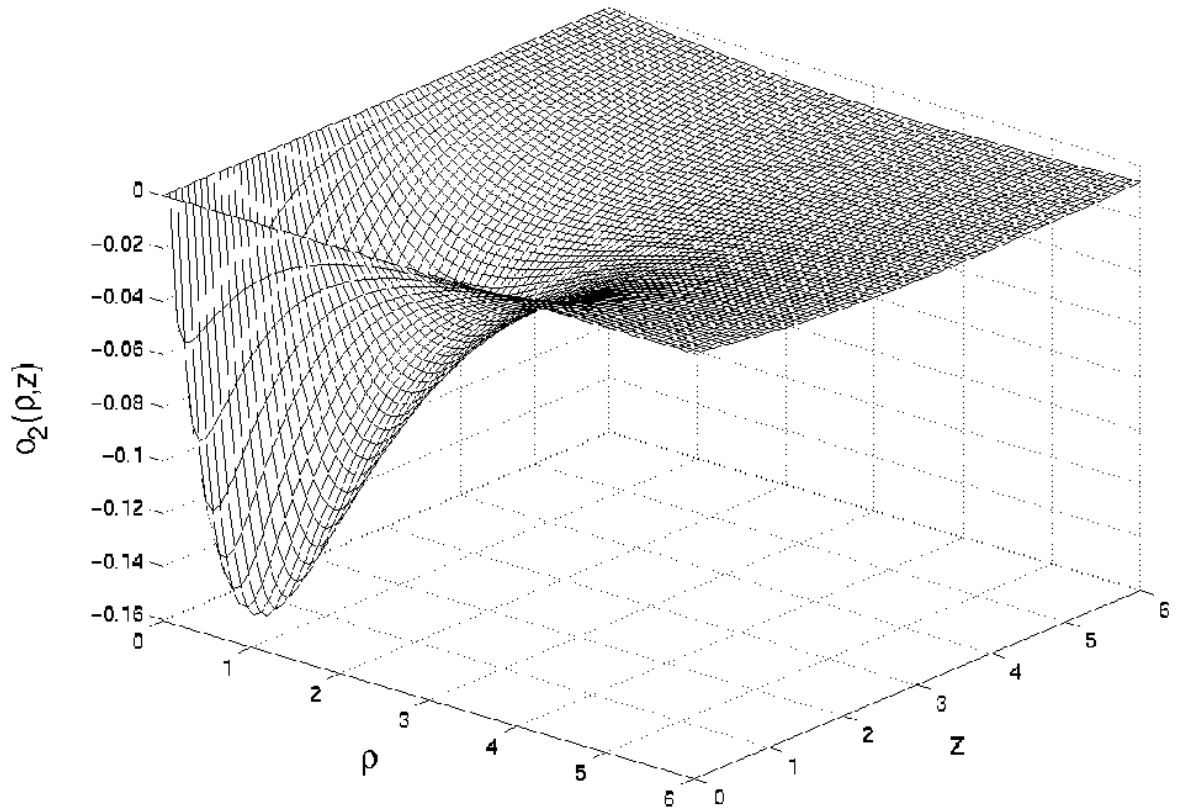


Fig. 7a

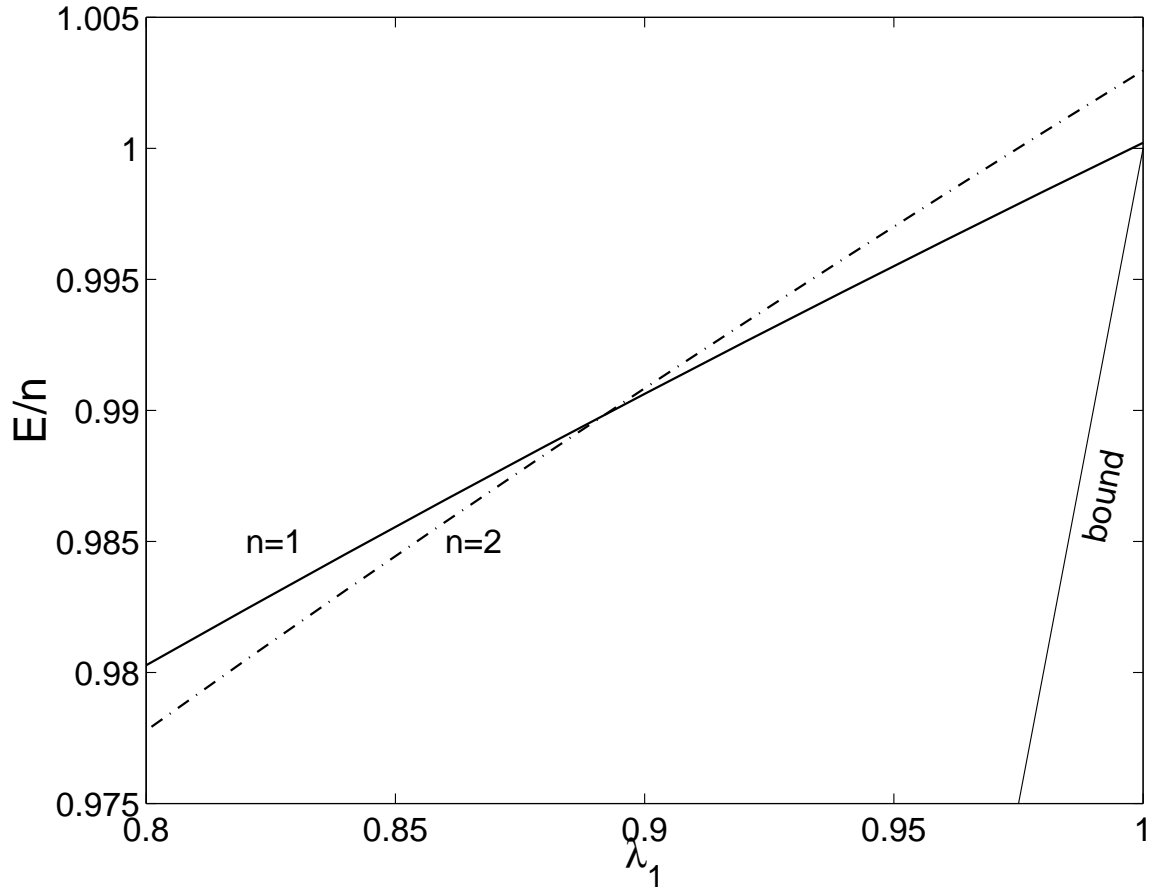


Fig. 7b

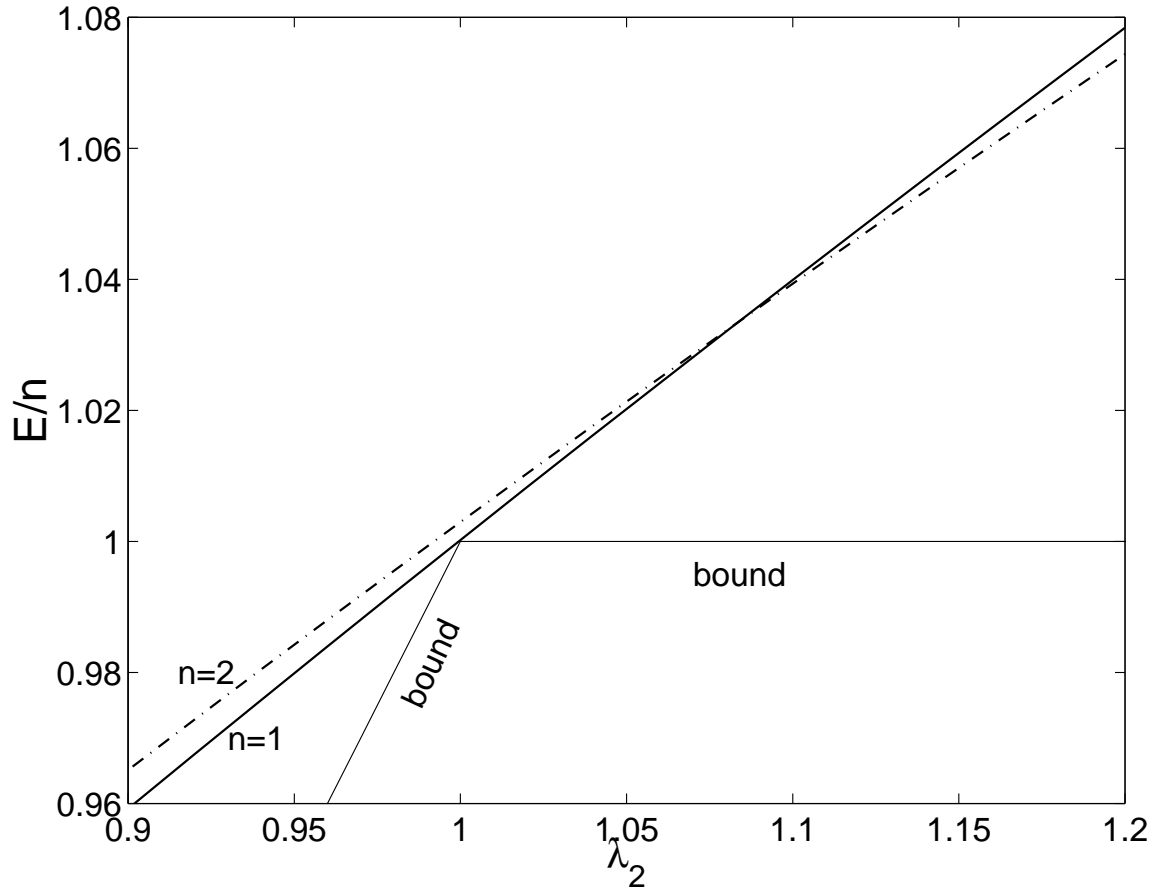


Fig. 7c

